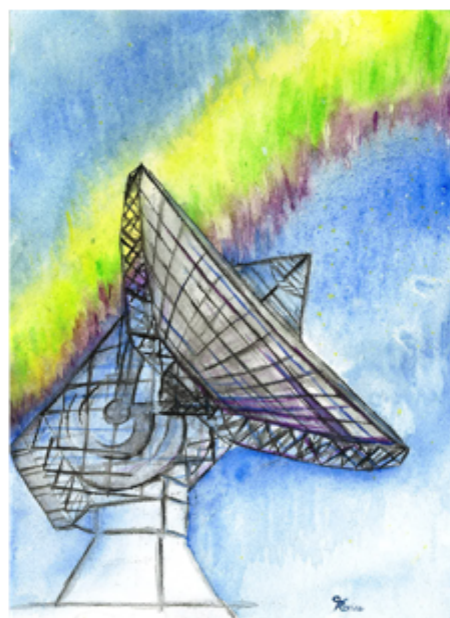




DEGREE PROJECT IN ELECTRICAL ENGINEERING,
SECOND CYCLE, 30 CREDITS
STOCKHOLM, SWEDEN 2019

On the Relationship Between Energetic Electron Precipitation and Mesopause Temperature

FLORINE ENENGL



KTH ROYAL INSTITUTE OF TECHNOLOGY
SCHOOL OF ELECTRICAL ENGINEERING AND COMPUTER SCIENCE

1. Abstract

Energetic Particle Precipitation (EPP) can potentially change the neutral atmospheric temperature at the mesopause region. Cresswell-Moorcock et al. (2013) used European Incoherent Scatter Scientific Association (EISCAT) radar data to identify strong electron precipitation events. Here we use a similar approach and search for electron precipitation events to investigate the simultaneous and co-located neutral temperature measurements. The temperature of the excited hydroxyl (OH) molecules is representative for the neutral air temperature at the height of the OH layer, assuming there is local thermodynamical equilibrium.

We use electron density datasets from the EISCAT Svalbard radar ranging from a historical data set from the International Polar Year (IPY) in 2007-2008, when EISCAT Svalbard radar was run continuously, up to February 2019. Following Cresswell–Moorcock et al. (2013) particle precipitation events are characterized by a rapid increase of the electron density by a factor of 5 at an altitude range of 80-100 km. To determine the neutral temperature, we use airglow data. Spectrometer measurements of OH airglow are collected at Kjell Henriksen-Observatory (KHO), only about 1 km away from the radar site. The neutral temperatures are averaged over one hour and half an hour and are available since the IPY.

The study shows different temperature responses to EPP, which are classified accordingly. Most events show an initial decrease in the order of 20 K. The temperature decrease may mean that the EPP ionisation changes the chemical composition in the mesosphere and decreases the population of excited OH at the top of the layer. As a consequence, the airglow peak height changes and the temperatures are probed at lower altitudes. Sporadic E-layers were additionally captured by the automatic routine to search for electron density enhancements and were examined separately. The response of sporadic E-layers on the mesopause temperature at the onset is comparable to the ones for EPP, even though the decrease in temperature is smaller than for EPP.

2. Sammanfattning

Energetisk partikelprecipitation (EPP) kan potentiellt ändra atmosfärstemperaturen i mesopausområdet. Cresswell-Moorcock et al. (2013) använde radardata från European Incoherent Scatter Scientific Association (EISCAT) för att identifiera fall av stark elektronprecipitation. Här använder vi ett liknande tillvägagångssätt. Temperaturen hos exciterade hydroxylmolekyler (OH) är representativ för temperaturen av den neutrala atmosfären vid OH-skiktets höjd, förutsatt att lokal termodynamisk jämvikt gäller.

Vi använder observationer av elektrontäthet med hjälp av EISCAT Svalbardradar från och med ett historiskt dataset från det internationella polaråret (IPY) 2007–2008, fram till februari 2019. Som hos Cresswell-Moorcock et al. (2013), kännetecknas fall av elektronprecipitation av en snabb ökning av elektrontätheten i ett höjdintervall av 80–100 km. För att bestämma den neutrala atmosfärens temperatur använder vi observationer av luftsken (engl. Airglow). En spektromätare observerar spektra av OH-luftsken vid Kjell Henriksen-observatoriet (KHO), endast cirka 1 km från radarplatsen. Temperaturdata kan fås från spektra medelvärdesbildade en timme, samt en halvtimme och är tillgängliga sedan IPY.

Studien visar olika temperaturreaktioner på EPP. De flesta händelserna visar en initial minskning i storleksordningen 20 K. Temperaturminskningen kan innebära att EPP-joniseringen förändrar den kemiska kompositionen i mesosfären, vilket minskar populationen av exciterad OH vid toppen av skiktet. Som en konsekvens förändras topphöjden för airglow och temperaturer mäts vid lägre höjder. Sporadiska E-skikt fångades dessutom av den automatiska rutinen för att söka efter elektrondensitetsförbättringar och undersöktes separat. Reaktionen av sporadiska E-skikt på mesopausstemperaturen vid starten är jämförbar med de för EPP, även om temperaturminskningen är mindre än för EPP.

3. Acknowledgements

This thesis has been carried out under supervision of Noora Partamies (University Centre in Svalbard) and Nickolay Ivchenko (KTH Royal Institute of Technology). I would like to thank Noora who not only truly inspired me with her motivation for research, but also with her knowledge as a scientist. I have found a role model in her to look up to. I would like to thank Nickolay who is a great mind and just impressive, as everyone knows. I am grateful to have learned from you! I would also like to thank Fred Sigernes for the OH data used in my thesis.

Furthermore, I want to thank Sydney Le Cras. I am glad we could spend some more time in Svalbard together - it felt like no time has passed since last time we have been here. There are several groups of friends I would like to thank specifically, as the Knitting B's, my study friends, Sjøskrenten 3rd floor and the Sushi Monday's group. Big thanks to FECE KEBF. Thanks to Nikolaus Huber for all the fun we always have.

I especially want to thank my partner William Janurberg, who I met during my Electrophysics studies and who always supports me. You make my life even happier. Finally, I want to thank my parents, Ingrid and Klaus Enengl, for enabling me to follow my interests and always supporting me. I am thankful for my sister, Iris Enengl, who completes me, which I named the radar experiment for this thesis after (ESIRI). Thank you to the cats in our family for always making me laugh. I am grateful to have done my thesis at the University Centre of Svalbard, Figure 3.1 captures my appreciation of Svalbard.



Figure 3.1.: Aquarelle painting of the office view, by Florine Enengl

Contents

1. Abstract	b
2. Sammanfattning	c
3. Acknowledgements	d
4. Introduction	1
4.1. The Earth's Plasma Environment	1
4.2. The Atmosphere	1
4.3. Research Question and Outline	2
4.4. Previous Studies of EPP effects on the Mesopause Region Temperatures	3
5. Background	5
5.1. Geomagnetic Field	5
5.1.1. Plasma Populations in the Inner and Middle Magnetosphere	6
5.1.2. Geomagnetic Disturbances	7
5.2. Particle Precipitation into the Atmosphere	8
5.3. Airglow	9
6. Instrumentation	11
6.1. Electron Density and Electron Temperature Measurements	11
6.2. EISCAT Svalbard Radar (ESR)	11
6.3. Ebert-Fastie Spectrometer	13
6.4. OH Rotational Temperature Measurements	13
7. Observations	15
7.1. EISCAT Svalbard Radar Datasets	15
7.2. ESIRI	15
7.2.1. Energetic Particle Precipitation	16
7.2.2. Sporadic E-layers	21
8. Analysis	22
8.1. Processing the Radar Data Set	22
8.2. Criteria for Energetic Particle Precipitation Events	23
8.3. Sorting of the Events into Different Categories	23

9. Results	25
9.1. Energetic Particle Precipitation Events	25
9.1.1. Events with Full Coverage of Temperature Data (Hourly Resolution) . .	25
9.1.2. Events with Partial Coverage of Temperature Data (Hourly Resolution)	33
9.1.3. Events with Full Coverage of Temperature Data (Half-Hourly Resolution)	35
9.1.4. Events with Partial Coverage of Temperature Data (Half-Hourly Resolution)	42
9.2. Sporadic E-layers	44
9.2.1. Events with Full Coverage of Temperature Data (Hourly Resolution) . .	44
9.2.2. Events with Partial Coverage of Temperature Data (Hourly Resolution)	46
10. Discussion	48
10.1. Discussion on EPP Effects on the Mesopause Temperature	48
10.2. Discussion on Sporadic E-layer Effects on the Mesopause Temperature	51
11. Conclusion and Outlook	53
12. Acronyms	54
A. APPENDIX	55
A.1. ESIRI experiment	55
A.2. Matlab codes	64
A.2.1. Reading in the EISCAT Data	64
A.2.2. Finding the Events	66
A.2.3. Electron Density and Airglow Temperature Event Plots	69
A.2.4. Scatter Plot	73
A.2.5. Superposed Epoch Plot	74
A.3. Sporadic E-layer Events Electron Density Plots: Cases with Full Temperature Coverage (Hourly Resolution)	76
Bibliography	78

4. Introduction

The effects of energetic particle precipitation (EPP) on the upper neutral atmosphere are the main theme of this thesis. This chapter presents the general background of the work, specific research questions, and a short survey of related research.

4.1. The Earth's Plasma Environment

The heliosphere is the region which is influenced by the sun and it moves with the sun through interstellar space. The sun's energy production is shaping the heliosphere and with it our plasma environment. The heliosphere is primarily subject to the sun's radiative, particulate and magnetic output. The sun's magnetic field is called the interplanetary magnetic field (IMF). The continuous stream of emitted plasma from the sun is named the solar wind. The IMF interacts with the earth's magnetic field and shapes an area around the earth, called the magnetosphere, see Figure 4.1 [1]. The magnetopause is the boundary between the solar wind and the earth's magnetic field. The magnetotail is formed on the night side region in the magnetosphere, see Figure 4.2. Within the magnetosphere, the magnetopause and the magnetotail there are electrical current sheets and different plasma populations.

Interaction of solar wind with the magnetosphere of the earth gives rise to a wide range of phenomena, for example, magnetospheric substorms and EPP. These phenomena may affect infrastructure, which includes our communication and navigation systems and power grids. In this case, they are referred to as space weather. Forecasting of space weather requires research from the sun to earth to improve the models used for the space weather forecasting simulations.

4.2. The Atmosphere

Understanding climate change requires advanced models of the atmosphere to describe its circulation and energy balance. Magnetospheric phenomena can affect the dynamics of the atmosphere by energy deposition in its upper layers. The atmosphere consists of different layers, each of these layers correspond to a specific altitude range where common characteristics of that layer are found, such as the temperature variation. The stratosphere and the mesosphere are called the middle atmosphere. The mesosphere is a region from about 50 km to about 85 - 90 km where the vertical temperature gradient is negative. The boundary between the mesosphere and the thermosphere is called mesopause [2]. Its altitude is subject to seasonal variation. The mesopause gets as low as 86 km in summer, and up to



Figure 4.1.: Aquarelle painting of the IMF interacting with the geomagnetic field shaping the magnetosphere, by Florine Enengl

103 km in winter [3]. In this thesis, the mesopause region is defined from an altitude of 80 to 100 km to include most of the measurement range of the hydroxyl (OH) peak altitude [4].

The ionosphere is a region where charged particles are found, the ionisation effects are dominant. The ionosphere is part of the upper atmosphere and starts above the middle atmosphere. The mesopause region is at the lower boundary of the ionosphere and the upper boundary of the neutral atmosphere [2]. The behaviour of neutral gas and ionized particles differ, that is why complex interactions between dynamics, photochemistry, heating and transport mechanisms take place and influence the energy budget in the region.

4.3. Research Question and Outline

The thesis is about characterizing the EPP effects in the ionospheric D-region, in particular the effects of EPP on the mesopause temperature. This is done by using the incoherent scatter radar data for determining the parameters of the ionospheric plasma and using airglow optical observations for determining the temperature of the neutral atmosphere. This thesis first presents the background and the instrumentation, describes the observations and analysis to then show and discuss the results.

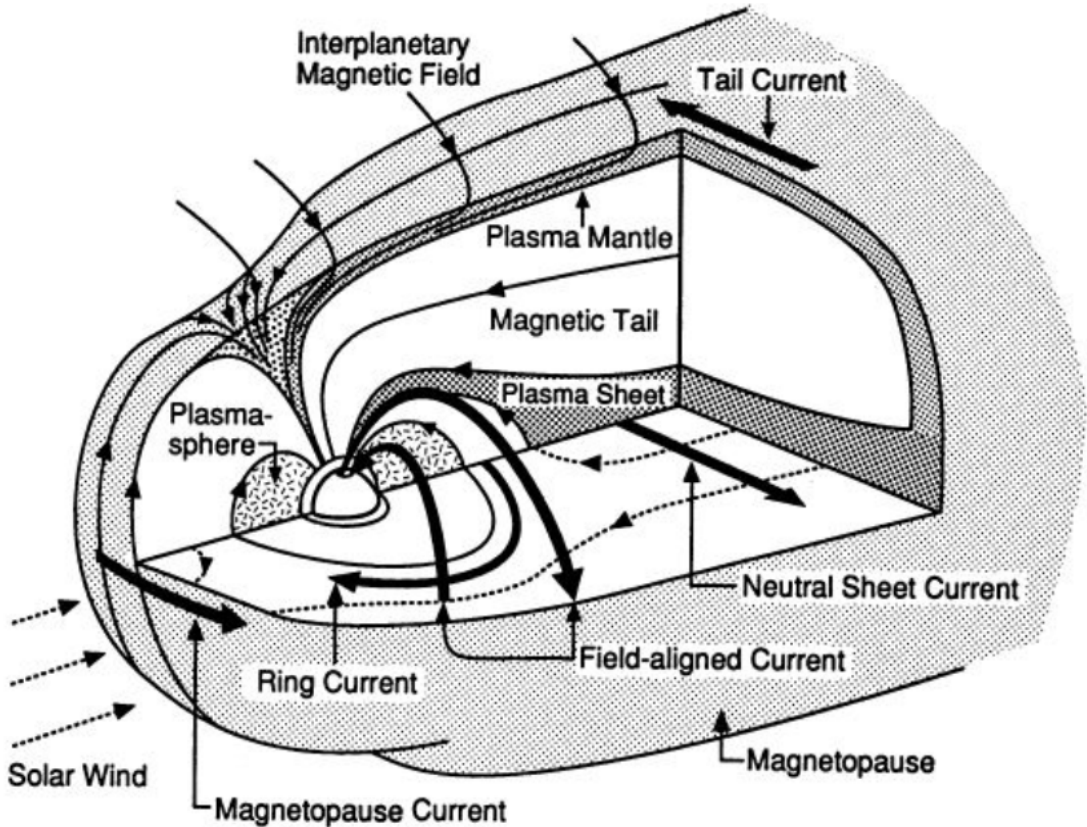


Figure 4.2.: Earth's magnetosphere and its plasma populations [5]

4.4. Previous Studies of EPP effects on the Mesopause Region Temperatures

Several studies have looked into the effects of EPP on neutral temperatures. H. Nesse Tyssøy et al. [6] compared particle precipitation observed by NOAA satellites with neutral temperatures derived from the TIMED satellite. They used a dataset of 80 days within May/ June and October/ November 2003 in the northern hemisphere and found temperature increases at all heights above 100 km. As EPP events change the Pedersen conductivity, Joule heating may contribute to the found temperature changes in these altitudes. In lower layers, a possible temperature decrease at around 90 km was found.

The OH rotational temperature during an aurora event was observed by H. Suzuki et al. [7] with the temperature measurements recorded at Syowa Station Antarctica by a high-sensitivity spectrometer. The relevant data set included 6 nights in 2018 in austral winter. In only one of these nights, an increase of the temperature and a decrease in intensity of OH airglow was found. They suggested a relation to EPP based on the horizontal magnetic field disturbance and a strong cosmic radio noise absorption.

4. Introduction

The connection of geomagnetic activity during the 23rd and the beginning of the 24th solar cycle and the mesopause region long term temperature changes was studied by Galina Gavrilyeva and Petr Ammosov [8]. The OH rotation temperature is used and assumed to be equal to the natural temperature at an altitude of 87 km. The average temperatures from 1999 to 2015 are included in the study. The results show that the mesopause temperature from October to February is about 10 K higher than in low activity years. The question on the relationship of EPP and the mesopause temperature is open.

5. Background

This chapter contains the background on the Earth's magnetic field, the plasma populations within and its disturbances, a description of particle precipitation into the atmosphere including its causes and effects, and the background of the airglow phenomenon.

5.1. Geomagnetic Field

The earth possesses an intrinsic magnetic field caused by a dynamo process in its liquid outer core. A simple approximation of the earth's magnetic field is a dipole field with its axis anti parallel and tilted about 11° to the rotational axis. The geomagnetic field has different contributors besides the dynamo and is subject to changes. The core field and the crustal lithospheric field are internal magnetic fields, whilst the external contributions come from the ionosphere and magnetospheric currents. The latter cause shorter variations of the geomagnetic field, whereas the dynamo is the reason for long-term changes [9].

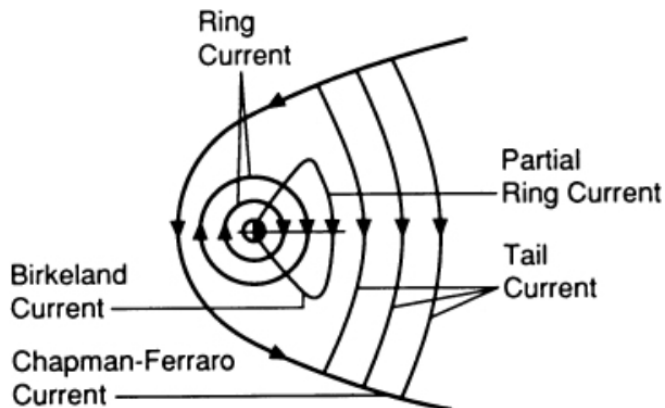


Figure 5.1.: Currents in the earth's magnetosphere in the equatorial plane as seen from above the north pole [5]

Currents within the magnetosphere are shown in Figure 5.1. The Chapman-Ferraro currents flow eastwards in the magnetopause. Magnetic field lines do not cross the boundary of the magnetopause. The tail current runs westward causing the magnetotail to be stretched. The ring currents flow westward around the earth, just as the partial ring currents. The partial currents of the middle magnetosphere are connected to the ionosphere through the Birkeland currents.

Currents within the geomagnetic field change the magnetic field. On the dayside the field strength is increased by the eastward Chapman-Ferraro currents. This causes a strengthening of the northward field, leaving the magnetopause compressed due to the solar wind. On the nightside the field strength decreases and the fieldlines of the magnetosphere close to the magnetopause turn equatorward and sunward along the magnetopause or poleward and tailward. Close to the earth's center (5 earth radii) the westward ring current causes the change of the field strength to be negative. The magnetic tail lobes field strength change is positive, caused by the westward tail current. These currents are controlled by the solar wind, its dynamic pressure and the electric field component [5].

5.1.1. Plasma Populations in the Inner and Middle Magnetosphere

Different major plasma regions are found in the inner and middle magnetosphere in the earth's magnetotail, the trapped radiation belts, the ring current region and the plasmasphere see Figure 5.2.

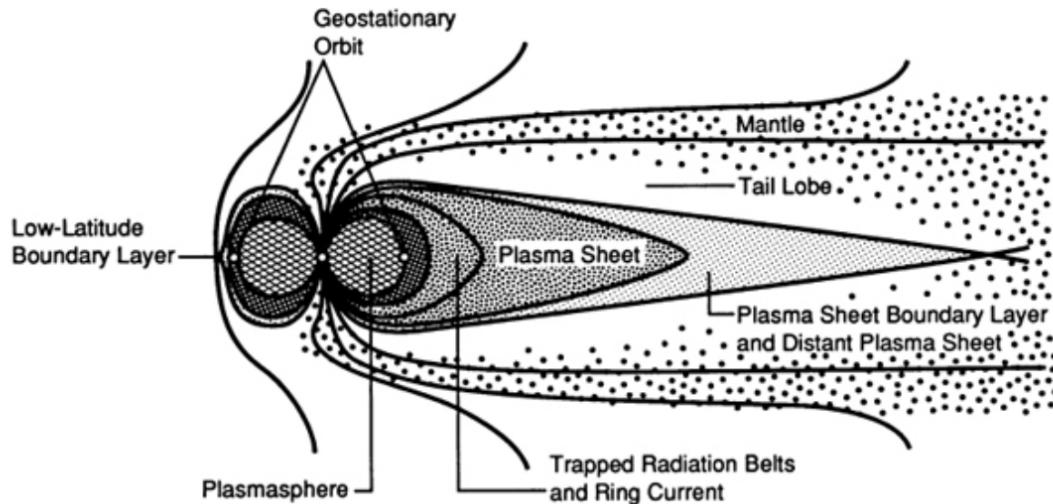


Figure 5.2.: Plasma populations in the earth's magnetosphere, view of the equatorial plane as seen from above the north pole with the sun at the left hand side [5]

The tail lobes within the magnetotail are regions of low density plasma, with a density less than 0.1 cm^{-3} . The plasma sheet boundary layer is found in between the lobes and the plasma sheet layer, with densities of around 0.1 cm^{-3} and is seen as a transition region between the low density lobes and the high density plasma sheet. The central plasma sheet's density is around 0.1 to 1 cm^{-3} . Reconnection in the tail redirects antisunward flowing plasma back to the earth. Strong magnetic activity causes the plasma sheet to move inside the geostationary orbit region, see Figure 5.3.

The geostationary orbit region is found at a distance of 6.6 earth radii in the equatorial plane. This is the region spacecrafts have their orbital periods equal to the earth rotation,

5. Background

staying in orbit around the earth at the same place. High magnetic activity can affect the spacecrafts in these orbits.

The radiation belts are found at a distance of approximately 6 earth radii. The trapped particles within the radiation belts carry the ring current. The particles are confined in the geomagnetic dipole field. Radial diffusion of protons and electrons and decay of neutrons are two of the mechanisms that feed the radiation belts. The particles in the belts are trapped in orbit around the earth and move mainly along the field lines and get mirrored. The particles can leave the belts dependent on their pitch angle to the magnetic field. The terms 'radiation belts' and 'Van Allen belts' include primarily the penetrating radiation, particles that penetrate deep into dense materials and can damage spacecraft instrumentation or harm humans. The ring current region includes all contributing particles and is the main contributor for external variations in the earth's magnetic field.

The plasmasphere region is made of dense and cold plasma situated in the same region as the radiation belts. High magnetic activity removes flux tubes from the outer plasmasphere [5].

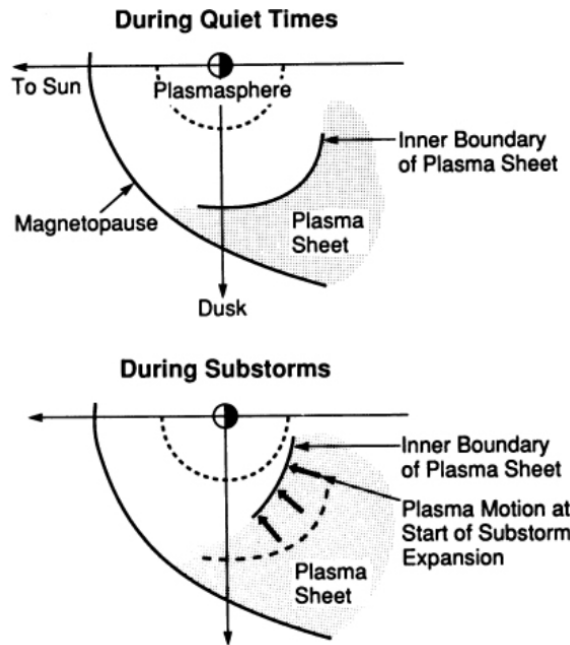


Figure 5.3.: Earthward moving plasma sheet during a substorm event, view of the equatorial plane as seen from above the north pole with the sun at the left hand side [5]

5.1.2. Geomagnetic Disturbances

When the solar wind properties change the currents change likewise. The earth's magnetic field responds to these variations and releases plasma into the inner magnetosphere or ionosphere as these disturbances occur. This is called geomagnetic activity. For reconnection

5. Background

to occur the field lines of the geomagnetic field must be antiparallel to the field lines of the solar wind, the IMF. For geomagnetic activity the IMF turns southward. For northward IMF activity is rarely found. The geomagnetic activity increases and decreases with the 11-year sunspot activity cycle. It also varies diurnally due to the earth's rotation [5].

Other non-periodical disturbances are called magnetospheric storms and magnetic substorms. Magnetic storms cause strongly perturbated conditions and happen when an intense coupling of the IMF and magnetosphere occurs over longer time. Magnetic storms have a duration from several hours to days. The intensity of the storms can be compared and identified by their value of equatorial horizontal (H) component of the magnetic field disturbance (Dst Index) [5] [10]. The storm threshold used for statistical studies can lie at - 50 nT, but even -30 nT could be chosen as a weak form. Big storms usually show a value of under - 200 nT. In between these, a storm is considered being intense, from - 100 to -200 nT.

Interplanetary coronal mass ejections (ICME) are large plasma ejections and magnetic clouds from the sun. ICMEs for example can cause magnetospheric storms going through the phases of storm sudden commencement, initial phase, main phase and recovery phase. The first phase happens when ICMEs are accompanied by a shock wave. It pushes in the magnetopause earthward, increasing the Chapman Ferraro current shielding the earth. If in the initial phase the IMF is southward the transition into the main phase happens fast. The main phase includes the start of the energy transfer to the ring current and tail current. In the mainphase the decrease of the H component happens. When the energy input decreases and the ring currents get weaker the Dst index returns to its usual values.

A magnetospheric substorm is a more frequent geomagnetic disturbance and has a duration of one to three hours. Substorms lead to an increase in the energy flow into the magnetosphere. They become partly visible as auroras. Substorms have a growth phase, a substrom onset, auroral breakup, an expansion phase and a recovery phase. The growth phase happens when the magnetotail field becomes stretched and it includes auroral arcs moving equatorwards and auroral electrojets. The substorm onset is when the most equatorward auroral arc brightens. The auroral breakup is the start of the expansion phase. In the recovery phase the magnetosphere and ionosphere recover to their quiet conditions [10].

5.2. Particle Precipitation into the Atmosphere

Precipitation of energetic particles from the magnetosphere into the atmosphere is mostly caused by loss processes, such as pitch angle scattering and charge exchange. Pitch angle scattering is the process by which the pitch angle distribution of a particle is modified. The particle with its the pitch angle α may be scattered into the loss cone. The loss cone angle α_{lc} is calculated using the adiabatic invariance of the magnetic moment μ which stays constant with

$$\mu = \frac{m \times v^2 \times \sin^2(\alpha)}{2 \times B} = \text{constant}. \quad (5.1)$$

5. Background

Using the energy conservation leads to

$$\frac{\sin^2(\alpha)}{B} = \text{constant}. \quad (5.2)$$

$$B_{turn} = \frac{B_0}{\sin^2(\alpha)}. \quad (5.3)$$

with B_{turn} at $\alpha_{turn}= 90^\circ$ when the particle turns and B_0 at α describing the magnetic moment before the turn at the magnetic mirror point.

Generally, the energy of a particle can only be reduced in the atmosphere and its first adiabatic invariant, the magnetic moment, is not conserved [11]. Particle Precipitation causing aurora has its primary source in plasma waves changing the particle pitch angles violating the first adiabatic invariant [5]. Whether a particle is lost or not depends on how deep in the atmosphere the point where magnetic field reaches this value lies. Commonly it is assumed that energetic particles are lost from the radiation belts into the atmosphere from an altitude of 100 km and lower. The loss happens by collision with atmospheric particles. Electrons with mirror altitudes above that are usually trapped. If a particle has its mirror point at or below 100 km it will be immediately lost into the atmosphere, this is named to be within the bounce loss cone. The height threshold in the bounce loss cone is also energy dependent [12] [13].

Therefore particles with pitch angles that are exceeding or equal to

$$\alpha = \arcsin\left(\frac{B_0}{B_{turn}}\right)^{\frac{1}{2}} \quad (5.4)$$

turn and particles with pitch angles lower than α are lost. Pitch angle scattering happens faster in the plasma sheet than in the radiation belts.

In the magnetosphere, also charge exchange causes loss of ions by

$$X^+ + Y = X + Y^+, \quad (5.5)$$

with X^+ being an energetic magnetospheric ion and Y a low energy neutral atom. This results in a low energy ionospheric ion Y^+ and an energetic neutral atom X which is no longer trapped as it is insensitive to the magnetic and electric fields [5].

Once energetic particles and solar photons reach the atmosphere they collide with atoms and molecules of the atmosphere, mainly nitrogen and oxygen. They ionize, dissociate, excite the particles in the atmosphere. An atom or molecule in an excited state, either decay into a lower energy state by emitting a photon or lose their energy in another collision. The characteristic green aurora is the strongest line of the spectrum at 557.7 nm, it is the decay of atomic oxygen, see Figure 5.4.

The processes change the composition of the atmosphere and the energy budget [14]. The EPP originates from cosmic rays, the sun or the magnetosphere.

5.3. Airglow

UV radiation from the sun is absorbed by molecular oxygen producing atomic oxygen. Oxygen is transported to lower altitudes, the mesopause region, by diffusion. It reacts and

5. Background

results in ozone, hydroxyl (OH) and active states of molecular oxygen [15]. Atmospheric photochemical processes or collisions excite these molecules and atoms. Their weak emission of light is called airglow. The visible airglow emissions during night, also called nightglow, come from atomic and molecular emissions of oxygen, metallic atoms and from vibrational-rotational bands of OH. The origin of dayside airglow is mainly resonance scattering, of the nightside airglow it is chemiluminescence of OH. Excited atomic oxygen emits photons with 557.7 nm and 630/636.4 nm wavelength at 90 to 100 km altitude and 150 to 300 km altitude. Sodium emits at 589 nm at around 91 km. Excited molecular oxygen emits at 310 to 500 nm at around 95 km. The vibrational-rotational OH emits visible to infrared radiation around 87 km altitude [16]. These layers are found globally at all times. The airglow intensities are used to obtain temperature measurements of the respective region. The mesopause temperature is determined by remote sensing measurements of the OH layer. The rotational temperatures of measured OH emissions can be derived by analysing the shape of the observed spectrum to be compared with the synthetic spectrum. It is assumed that the excited OH molecules are in a thermal equilibrium with the atmosphere, therefore the temperature is seen as the kinetic representative of this altitude in the atmosphere. The range of the OH peak altitude is measured to extend from 76 km to 90 km in Longyearbyen according to Mulligan et al. (2009)[4]. This region is a boundary between neutral atmosphere and the ionosphere and affected by EPP.

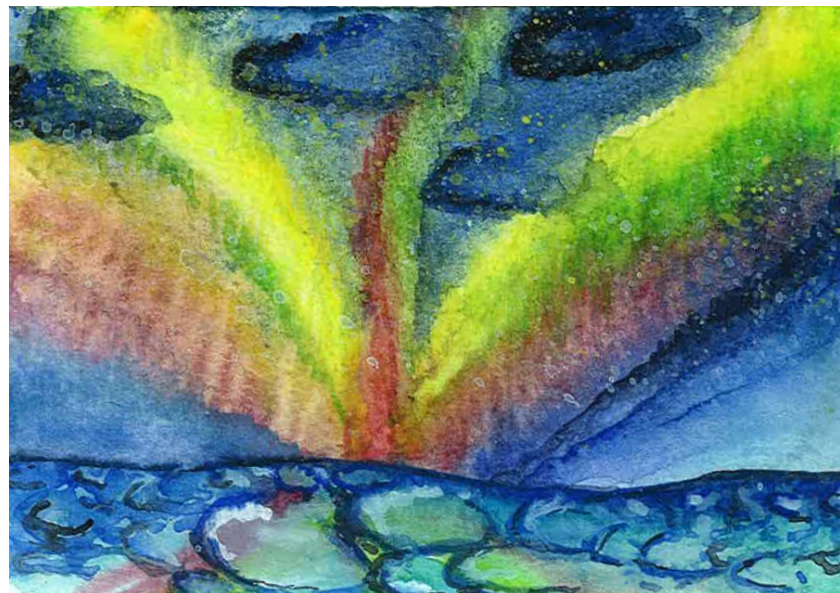


Figure 5.4.: Aquarelle painting of aurora over drift ice on Svalbard, by Florine Enengl

6. Instrumentation

In this chapter the measurement technique, retrieval of the electron density and temperature and instrumentation are explained.

6.1. Electron Density and Electron Temperature Measurements

Incoherent scatter is an electromagnetic wave weakly scattered by individual electrons with uncorrelated motion. The fluctuations in the plasma density of the ionized gas are caused by discreteness of electrons and ions and random thermal motion of the particles. The particles, which scatter the signal, have phases varying with time and are unrelated. This is based on Thomson scatter theory of electromagnetic waves on free electrons. Observational results showed that the Doppler broadening of the echo was less, as Thomson scattering does not include the influence of the ions. The Debye length D_e , with the electron temperature T_e and the electron density N_e is given by

$$D_e = 6.9 \times \frac{T_e^{\frac{1}{2}}}{N_e} [m] \quad (6.1)$$

, with N_e and T_e in SI units, and is the radius of a sphere around the positive ion in which electrons do not act independently, but are influenced by the heavier ion. Incoherent scatter is detected when the radar wavelength is bigger than or about the same as the Debye length.

The backscattered signal, from along the direction the radar is pointing, is received to an incoherent scatter radar. The power spectra of returned pulses is derived by autocorrelation and Fourier transformation. From this the frequency shift, the amplitude, width and shape of the spectrum is obtained. Out of these for example the electron temperature to ion temperature ratio, the electron density, the vector ion velocity, the ion composition as functions of height can be calculated. More parameters as the Hall and Pedersen conductivities, Joule heating, energy deposition by auroral electrons, neutral temperatures etc. can be conducted by assuming neutral densities in the plasma [17].

6.2. EISCAT Svalbard Radar (ESR)

EISCAT is an international scientific association conducting ionospheric and atmospheric measurements with radars. The facilities are found in Sweden, Finland and Norway. For this thesis the ESR in Longyearbyen, Norway is used. The peak power is 1000 kW. The radar operates in the 500 MHz band and has a 32 m steerable parabolic dish antenna and a 42 m

6. Instrumentation

fixed parabolic antenna aligned to the local geomagnetic field [18]. Datasets of the electron density measurements from both antennas are used for this thesis.

There are different experiments at EISCAT that can be run. The experiment is chosen dependent on the altitude of interest, see Figure 6.1. The experiments are a set of instructions to the transmitters, receivers and digital signal processing units to execute commands at different times. The altitude ranges and temporal resolutions of the experiments used in common programs are shown in table 6.1. Also special programs can be run as modifications of the existent experiments. The *manda* experiment offers good resolution in altitudes of 80 to 100 km and is therefore the choice for the radar runs specifically for this thesis. Additionally to *manda*, previous data sets of the *ipy* experiment are used, as it also covers the mesopause region. However, it has a lower spatial resolution. The *manda* experiment uses a single 32 m dish, *ipy*, *beata*, *tau7* are switchable between the 32 m and 42 m dish and *folke* uses both dishes. For this thesis the *manda* experiment on the 32 m dish and the *ipy* experiment on the 42 m dish are used.

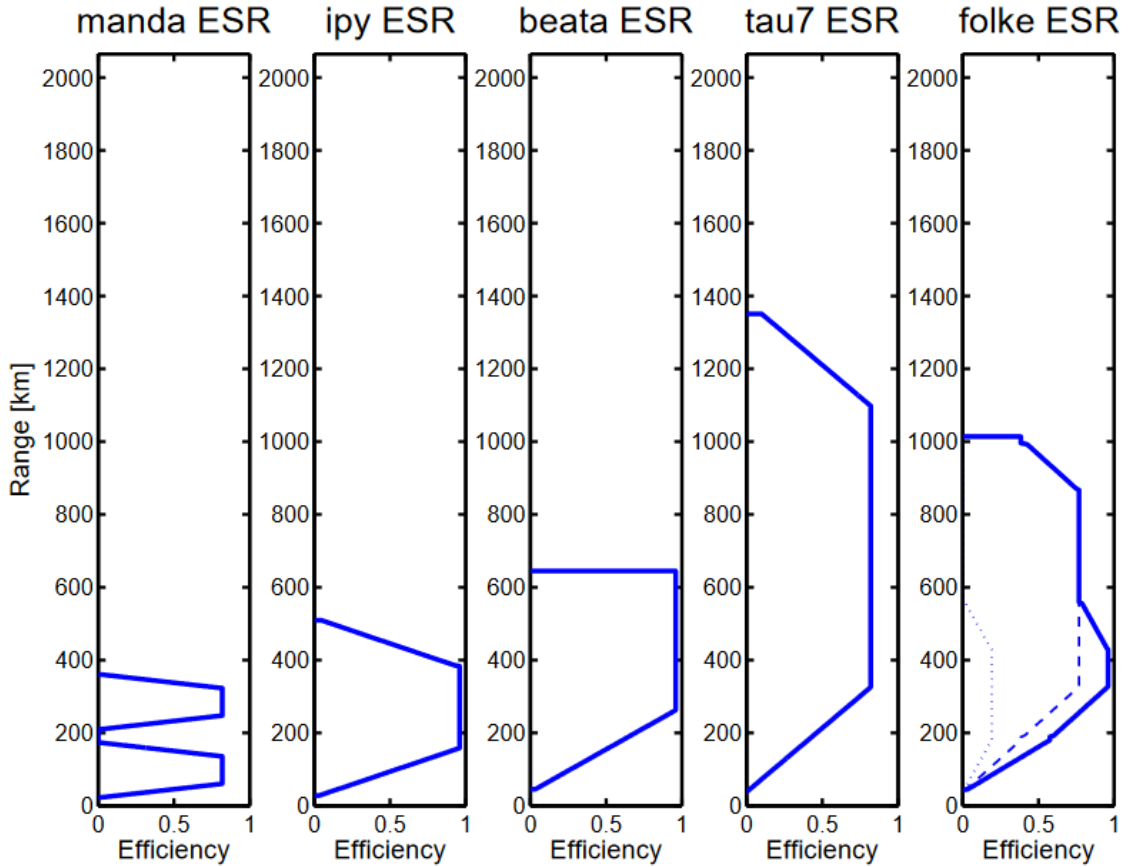


Figure 6.1.: Ranges covered by the ESR by different experiments [18].

6. Instrumentation

name	range span [km]	time resolution [s]	antenna dish [m]
<i>manda</i>	23-361	4.0	32
<i>ipy</i>	28-509	6.0	32, 42
<i>beata</i>	45-645	6.0	32, 42
<i>tau7</i>	39-1351	6.0	32, 42
<i>folke</i>	43-1014	6.4	32, 42
<i>dual folke</i>	43-555	6.4	32, 42

Table 6.1.: ESR experiments used in common programs range span, time resolution and antennas used [18]

6.3. Ebert-Fastie Spectrometer

The Ebert-Fastie Spectrometer at the Kjell Henriksen-Observatory in Longyearbyen, Svalbard is used to retrieve the winter temperature of the mesosphere. It scans the near infrared wavelength region, from 824 to 871 nm, this includes the rotational OH(6-2) band of the airglow. The spectrometer has a focal length of 1 m, points to zenith with a field of view of 5 degrees and a spectral resolution of 0.4 nm. One scan of the wavelength range takes 25 seconds but to obtain good signal-to-noise ratio several scans are averaged during post-processing of the data [19]. Most earlier studies use 1-hour averages. In this study half-hour averaging is examined in addition.

6.4. OH Rotational Temperature Measurements

The rotational OH temperature is seen as the neutral temperature of the mesopause region, assuming that its excited OH molecules are in thermal equilibrium with the atmosphere. The temperatures are derived from the intensities of the rotational OH lines. The lines can be measured by spectrometers. For a transition from an upper vibrational state v' and to a lower state v'' of the OH molecule $OH(v' - v'')$, the intensity I can be written as

$$I_{v',J' \rightarrow v'',J''} = N_{v',J'} \times A_{v',J' \rightarrow v'',J''}, \quad (6.2)$$

with the selection rule for the rotational state J : $\delta J = -1, 0, 1$. $N_{v',J'}$ stands for the number of molecules in the upper state. The Boltzmann distribution is used to determine it. A is the transition probability from state v', J' to state v'', J'' producing the line the intensity is measured from. N is a function of the rotational temperature. To retrieve the temperature the spectra are averaged hourly / half-hourly to keep the noise low. This results in a 144 / 72 counts per 1 h / 30 min integration time spectrum. Then the measured spectrum is fitted according to the emission lines at specific wavelengths in the synthetic spectrum. The resolution of the interpolation of the raw spectrum to fit the synthetic spectrum is 0.1 nm. Due to the split of the OH ground state the rotational transitions produce emission line doublets, P1 and P2. Through a linear fit of the P1 and P2 emission lines the background is subtracted

6. Instrumentation

from the peak values of the intensities of the rotational lines in order to obtain the relative intensities of the different emission lines, see Figure 6.2. The slope of the best fit is used to find the temperature value. The result of the fitting is the temperatures, the background level, the slope, the covariance of the measured and synthetic spectrum, the variance of the intensity lines from the linear fit and the relative intensity [20].

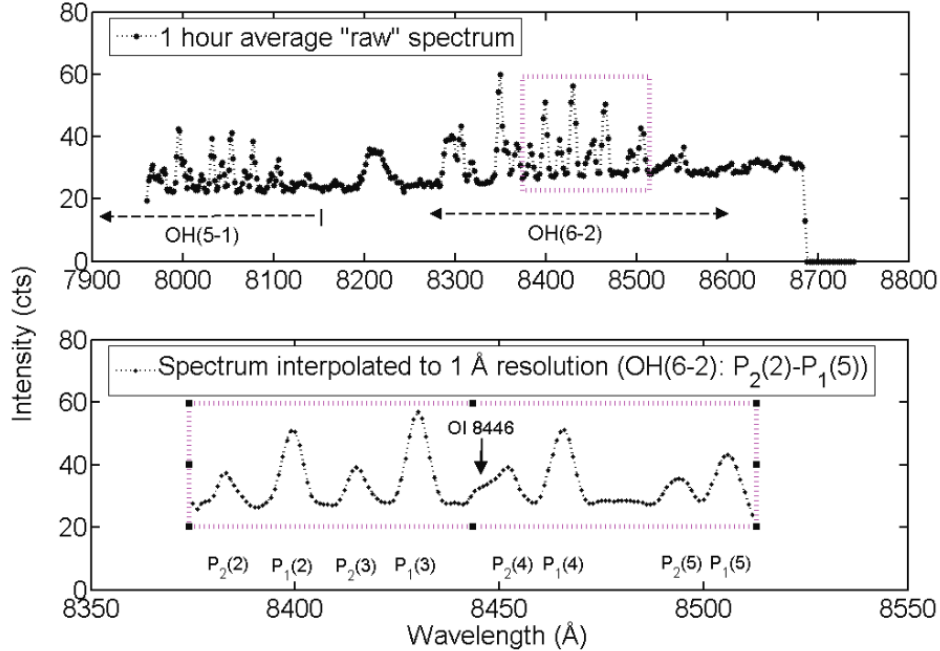


Figure 6.2.: The top panel of the Figure is an hourly averaged spectrum before the interpolation. The analysed wavelength range is within the pink dashed rectangle in both panels. The bottom panel shows the measured spectrum after the interpolation to 0.1 nm resolution. The spectrum is fitted to the P1 and P2 emission lines [20].

7. Observations

7.1. EISCAT Svalbard Radar Datasets

For this thesis a total of 10220 hours of EISCAT data are analyzed. 10144 of these are from *ipy* experiments and 76 hours from *manda* experiments. *ipy* and *manda* are chosen as their spatial resolution is sufficient to detect enhanced electron densities in the mesopause altitude range. Only experiments with an elevation of $90^\circ \pm 10^\circ$ are chosen for this data set. As the 42 m dish of the ESR is fixed pointing to the local geomagnetic field, *ipy* runs on the 42 m dish are included and the scans with the moving 32 m antenna of the *ipy* runs are excluded. The data set starts at the International Polar Year 2007/08 when the ESR had been run continuously from 1st of March 2007 to 29th of February 2008. This year includes 8784 hours in the *ipy* experiment mode. Additionally to this data, *manda* and *ipy* experiments from December, January and February every year until February 2019 are included in the analysis. This covers a full solar cycle. The ESIRI experiment (ESR Ionospheric D-Region Experiment for Investigation of EPP) was run in the experiment mode *manda* for a total of 48 hours in January and February 2019 to specifically collect data for this thesis. The data collected during the ESIRI experiment is described further in this chapter. The analysis of the radar data is discussed in the next chapter.

7.2. ESIRI

The *manda* experiment was run for a total of 24 hours in January 2019 and 24 hours in February 2019. The 48 hours are split up in 8 evening runs from 16 to 22 UT each. The cases with clear electron density enhancements in the mesopause due to electron precipitation are discussed in this section. In addition, some sporadic E-layers also occurred. They were unexpected in EPP search but are a known phenomenon. Both event types are further discussed in the following sections. Appendix A.1 contains all electron density plots for the ESIRI experiment. Solar wind data (magnetic field strength, solar wind velocity) for these runs has been downloaded from the NASA OMNIWeb Data, which is based on satellite measurements, accessible from https://omniweb.gsfc.nasa.gov/form/omni_min.html. The auroral electrojet index is accesible from <http://wdc.kugi.kyoto-u.ac.jp/aedir/> and provides a global and quantitative measure of auroral zone magnetic activity from enhanced Ionospheric currents flowing below and within the auroral oval.

7.2.1. Energetic Particle Precipitation

EPP events are found by an increase in the electron density penetrating from high to low altitudes. The electron density during the radar run on the 5th of January is shown in Figure 7.1. Visual inspection shows EPP events commencing at 21:50 UT on the 5th and at 19:50 UT on the 6th of January. In this case the background electron density values lie at a magnitude of $5 * 10^9 m^{-3}$ and at the event onset change to over $10^{10} m^{-3}$ in the mesopause region. The solar wind magnetic field data for the 5th of January is shown in Figure 7.2. The magnetic field magnitude average (Bmag) from 16:00 to 22:00 UT, shown in the first panel, stays around a mean of 6.8 nT, with a standard deviation of 2.6 nT. The second panel shows the solar wind magnetic field in z direction (Bz) turning southwards from 18:27 UT to 19:23 UT and again 20:02 to 22:22 UT. The third and forth panel show the hourly and half hourly OH rotational temperature during the radar run. The last panel shows the auroral electrojet index. The mean solar wind velocity (not shown) from 16:00 UT to 22:00 UT is 486.5 km/s, with a standard deviation of 34.1 km/s. The auroral electrojet index is increased from 17:00 UT to 21:00 UT, but stays low at the EPP occurrence.



EISCAT Scientific Association EISCAT SVALBARD RADAR

RT, 32m, manda, 5 January 2019

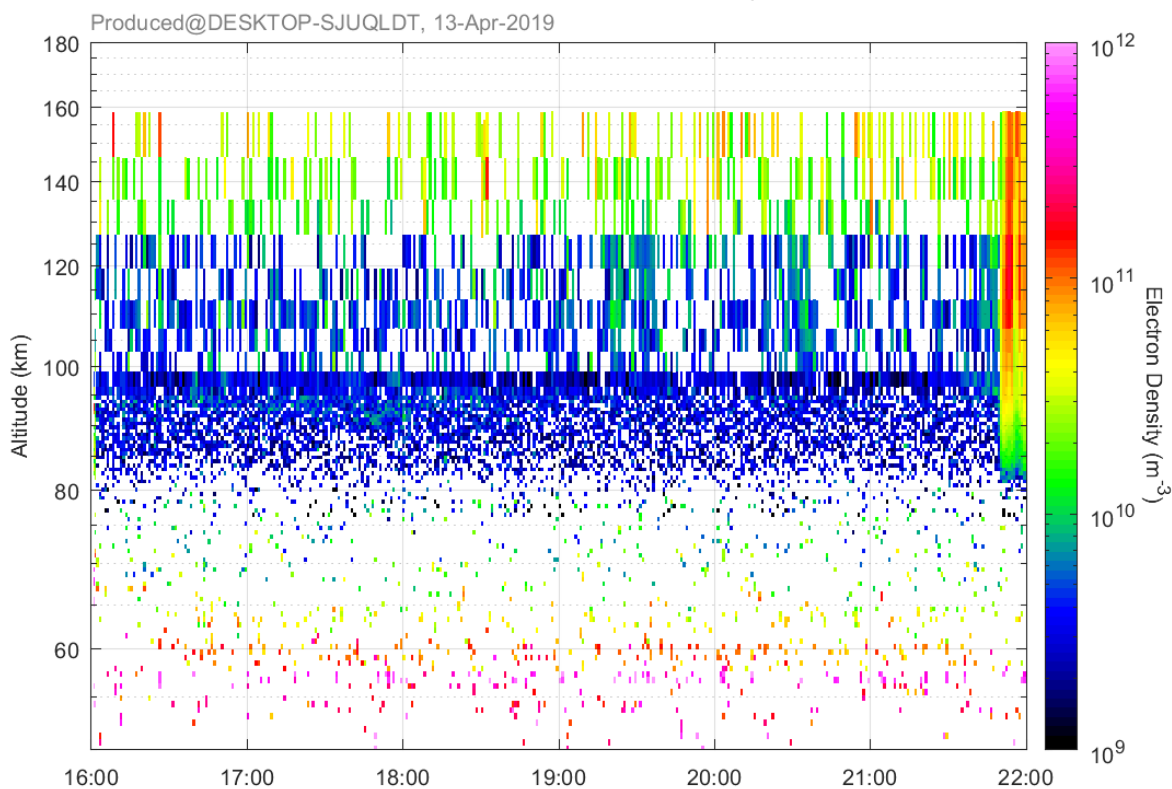


Figure 7.1.: electron density plot versus altitude and time for the *manda* experiment on the 5th of January 2019, 1600-2200 UT, altitude range shown: 50 to 180 km; particle precipitation event found at 21:50 UT

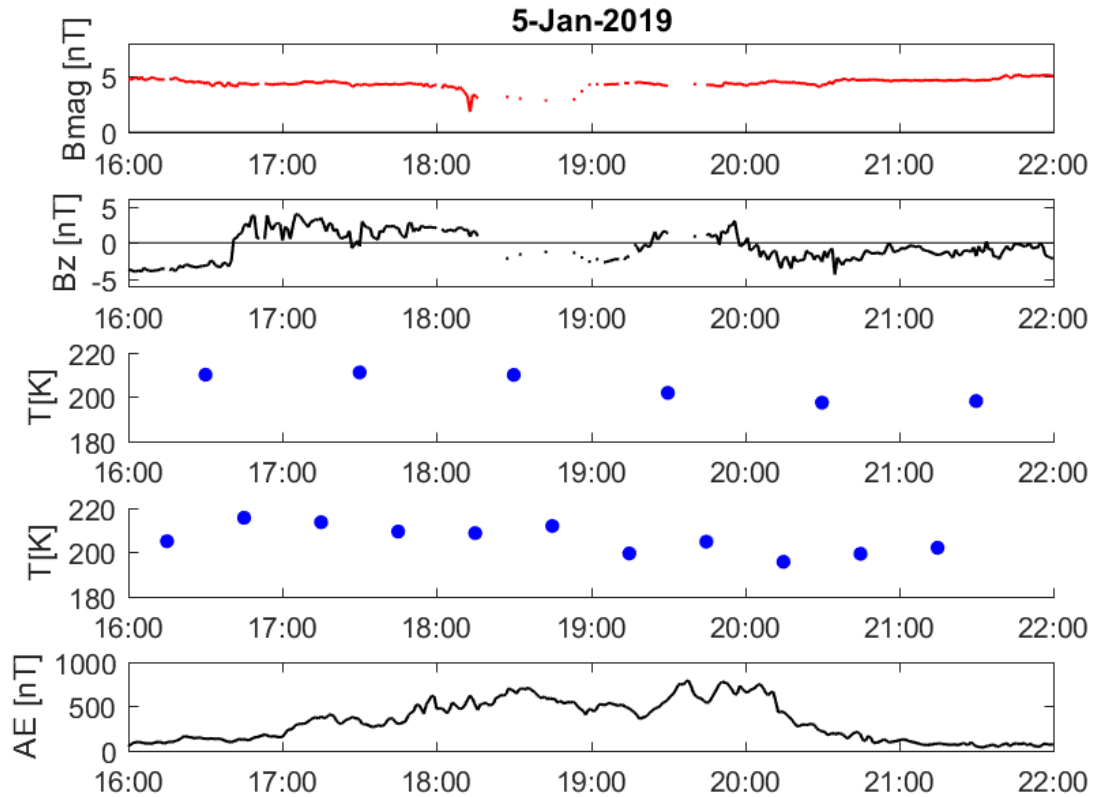


Figure 7.2.: Bmag, Bz are shown from 16:00 UT to 22:UT on the 5th of January 2019. The third panel shows the hourly OH rotational temperature values during the radar run, the forth panel the half-hourly resolution OH rotational temperature data and the last panel the auroral electrojet index.

7. Observations

The electron density variations on the 6th of January from 16:00 UT to 22:00 UT are shown in Figure 7.3. The onset of the EPP is at 19:50 UT. Figure 7.4 shows Bmag, Bz, the OH rotational temperatures and the auroral electrojet index. The mean value of Bmag from 16:00 UT to 22:00 UT is 4.8 nT with a standard deviation of 0.8 nT. The Bz turns southward from 16:44 UT to 17:13 UT and 17:23 UT to 19:25 UT and is then mostly negative from 20:14 UT to 22:02 UT. The mean solar wind velocity (not shown) from 16:00 UT to 22:00 UT is 522.2 km/s with a standard deviation of 22.6 km/s. The OH rotational temperature is shown in the third and forth panel and the auroral electrojet index in the last panel of 7.4. The auroral electrojet index stays low at the EPP event. The solar wind speed and the magnitude of the magnetic field stay stable for both events.



EISCAT Scientific Association

EISCAT SVALBARD RADAR

RT, 32m, manda, 6 January 2019

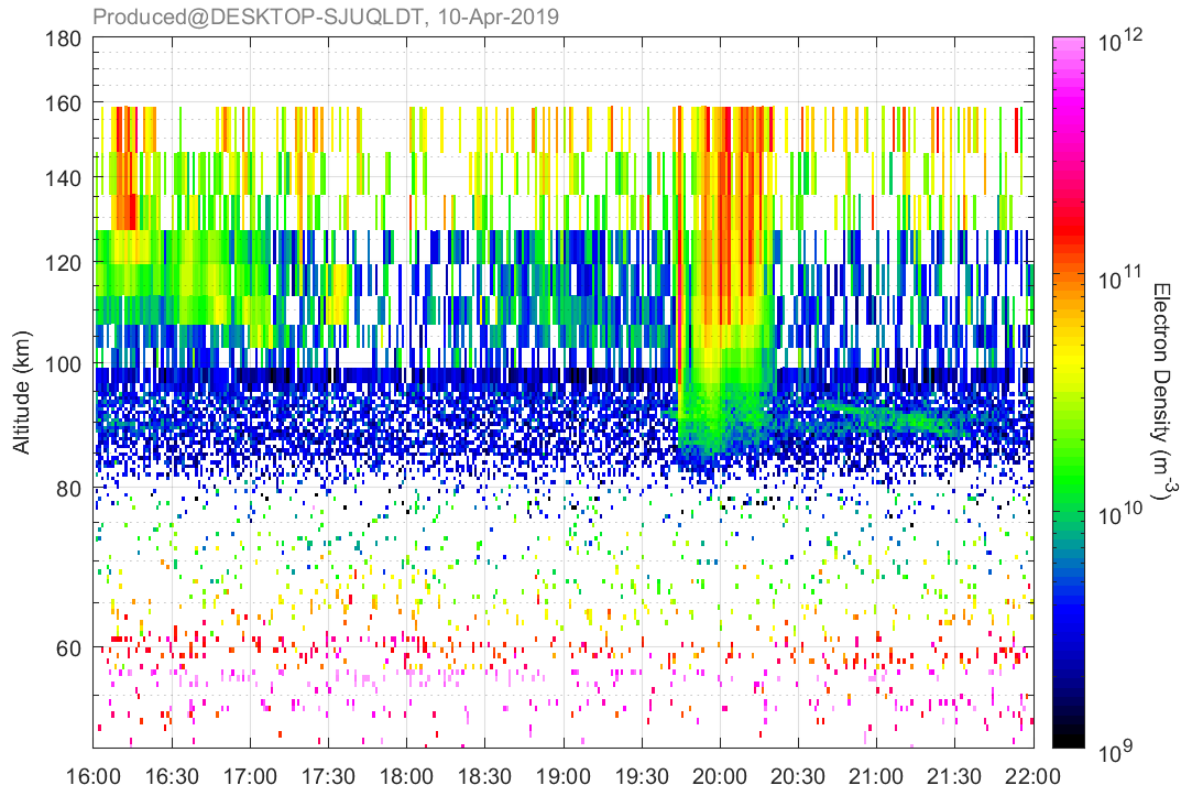


Figure 7.3.: Electron density plot versus altitude and time for the *manda* experiment on the 6th of January 2019, 1600-2200 UT, altitude range shown: 50 to 180 km; particle precipitation event found at 19:50 UT

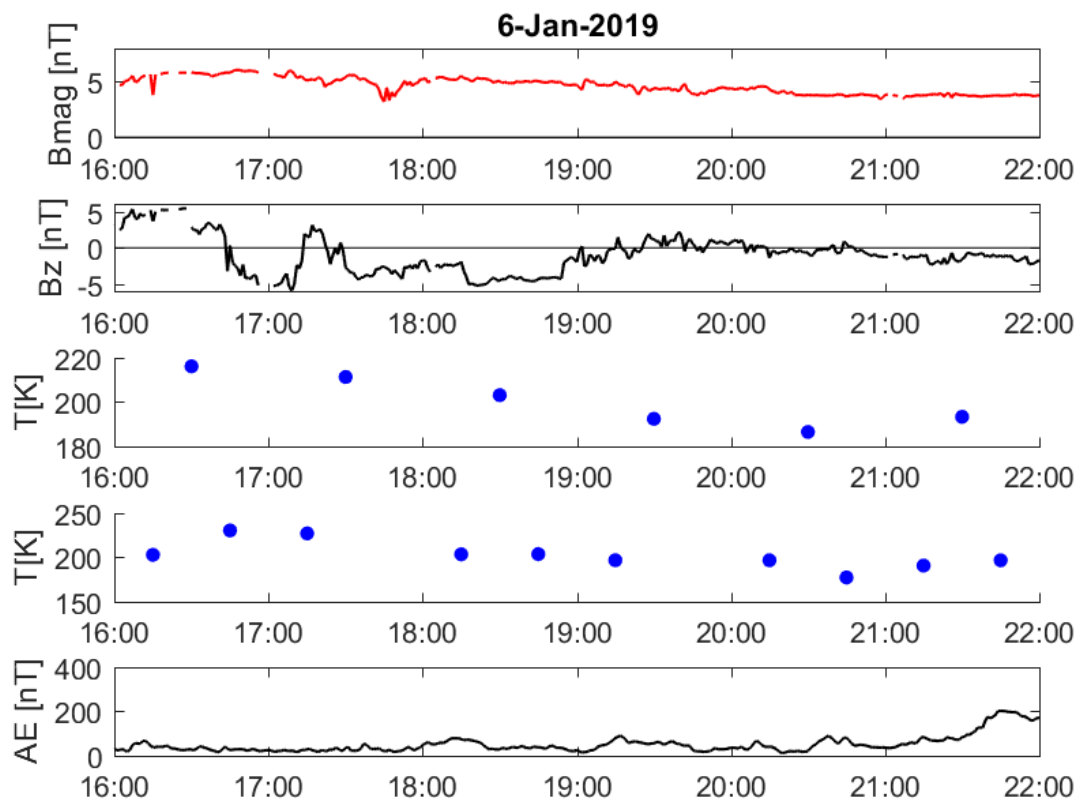


Figure 7.4.: IMF Bmag, Bz are shown from 16:00 UT to 22:UT on the 6th of January 2019. The third panel shows the hourly OH rotational temperature values during the radar run, the forth panel the half-hourly resolution OH rotational temperature data and the last panel shows the auroral electrojet index

7.2.2. Sporadic E-layers

Besides the EPP also sporadic E-layers in the altitude range of 80-100 km are found. A sporadic E-layer is a thin electron density enhancement at the E region at an unpredictable altitude and/or an unexpected intensity [21]. The anomalous values of ionization are confined within a limited thickness of a few kilometers. Sporadic E-layers occur between 90 and 130 km [22]. These enhancements can be seen on the plots of the 3rd and 4th of January 2019 and the 12th, 13th of February in Appendix A.1 and 14th of February 2019. The electron density plot for the 14th of February from 50 to 180 km altitude, Figure 7.5, shows vertical enhancements starting at 16:00, 17:40 and 18:50, the latter one reaches lower altitudes of 90 km and continues until the end of the radar run. The thickness of the layer varies between about 2 to 5 km.

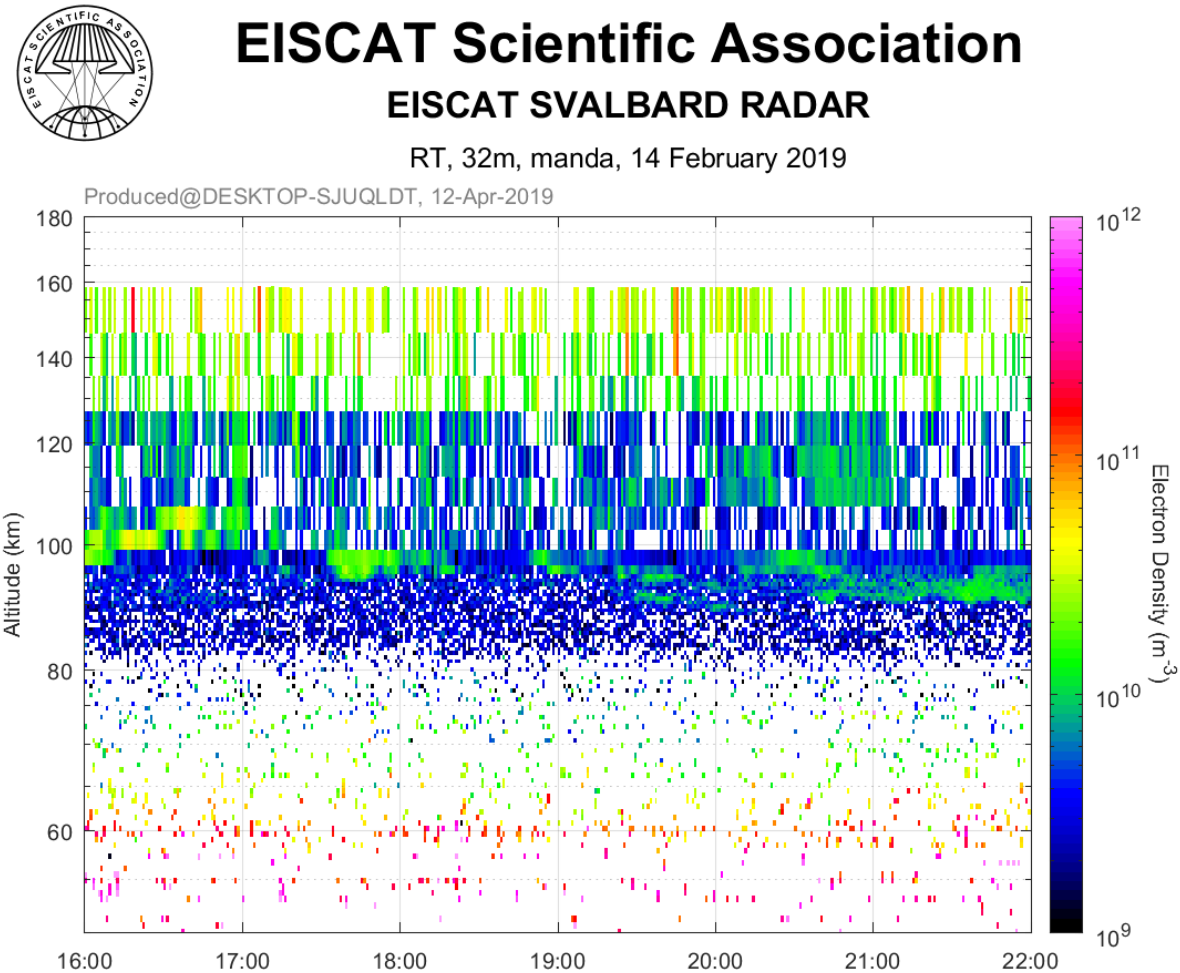


Figure 7.5.: electron density plot versus altitude and time for the *manda* experiment on the 14th of February 2019, 1600-2200 UT, altitude range shown: 50 to 180 km; sporadic E-layers visually inspected

8. Analysis

This chapter explains the steps from receiving the EISCAT radar data and rotational OH temperature data and processing the data sets to characterizing the EPP events and sorting the events into different categories.

The EISCAT raw data files can be accessed over the webpage: <https://www.eiscat.se/schedule/schedule.cgi>. Analyzing the raw data can be done by the Grand Unified Incoherent Scatter Design and Analysis Package (GUISDAP) system to perform full-profile analysis of incoherent scatter measurements. Instead of point values of plasma parameters, GUISDAP is designed to fit ionospheric profiles, which are no longer assumed to be slowly varying [23]. For selected experiments the GUISDAP analysed 1 minute resolution file can be downloaded. If the analysed data are not available online, GUISDAP can be used locally to produce analysed files in different resolutions. The product of the GUISDAP analysis are Matlab files for every minute, including the needed parameters for this thesis: the electron density parameter and its error, the altitude ranges and the integration timestamp of the file. For the airglow data sets the analysis as described in 6.4 is done twice, once for the hourly averaged temperature data and once for half-hourly resolution. Each airglow data set has a time vector, a temperature vector and a temperature error vector. For each version there is a different code to read in the files to set the time points for the temperature to the center over their averaged time.

8.1. Processing the Radar Data Set

The Matlab data files for 1-minute resolution are read into the Matlab code and for each file the end minute of the integration time is saved to generate a time vector, with the seconds set to zero. The time vector corresponds to the column indices of the electron density matrix. To assure a consistent electron density matrix for every minute the missing columns (minutes) are filled with NaNs. The time vector starts at the full hour in which the first electron density measurements of the experiments are registered.

Every Matlab data file also contains an altitude vector, which corresponds to the row indices of the electron density matrix. All data recorded at a specific altitude ± 0.5 km are averaged and stored as one corresponding value for this altitude. The height resolution of the experiment is bigger than 0.5 km, so there is normally just one value within that range. For *ipy* the data points within 80 to 100 km are recorded roughly centered at the altitudes 85 km, 89 km, 93 km and 97 km. It is chosen to average the altitudes from 87 to 90 km and from 91 to 94 km which also mainly includes one point per chosen altitude range.

Data from higher than 94 km is excluded as the range of the OH peak altitude is measured

to extend from 76 to 90 km in Longyearbyen [4] and above 94 km the found enhancements might not show a clear effect on the temperature. Any precipitation-enhanced electron density below 87 km would also affect the height range of interest above it, therefore the density measurements below are not included in the analysis. EPP shows electron density enhancements in the altitudes above the height of interest. The error of the electron density is read in and averaged to give a mean error.

Subsequently a 10 minute averaged electron density is calculated for the altitude ranges from 87 to 90 km and from 91 to 94 km . For the electron density time steps to be centered at every 10 minutes, the first average is build at 10 minutes past the full hour, where the time vector starts. For example the average for the timestamp minute xx:20 includes minute 16 to minute 25. The same is done for the electron density error. The code for reading in the EISCAT Data Set is found in Appendix A.2.1

8.2. Criteria for Energetic Particle Precipitation Events

The search for the EPP events in the radar data is based on Cresswell-Moorcock et al (2013) [24]. The onset is found by a sudden increase of the median electron density by a factor of 5 over 5 minutes [24]. For this thesis the electron density is averaged over 10 min with an altitude resolution of 4 km. The criterion was slightly adapted to find an increase of electron density by a factor of 4 within 20 minutes of the precipitation onset. If onsets are found only 10 minutes apart, the latter registered event is removed. The code for generating the EPP event list is found in Appendix A.2.2.

8.3. Sorting of the Events into Different Categories

The events are sorted by visual inspection of temporal evolution of the electron density and neutral temperature at the altitude the event is found. Electron density and neutral temperature are plotted from 3 h before to 3 h after the detected electron density enhancement as a function of time. One example plot is shown in Figure 8.1 (the rest in the appendic A.2.3). Events with large electron density errors are excluded. Cases with less than two temperature values within the time range are also excluded. Then the electron density data is plotted versus the altitudes 87 to 126 km versus the timespan from 3 h before to 3 h after the detected electron density enhancement. The events are inspected closer by looking at the altitudes above. Events that show a clear precipitation coming from upper altitudes are sorted into the EPP category. Events that show characteristics of sporadic E-layers as described in section 7.2.2 are sorted into the sporadic E-layer category. The remaining events not showing clear EPP or sporadic E-layer behaviour are taken out of the study. Finally, the events for which the temperature measurements are available within 1 h before and 1 h after the event are sorted into the full coverage category. The events for which the immediate temperature points are not available are sorted into an extra category.

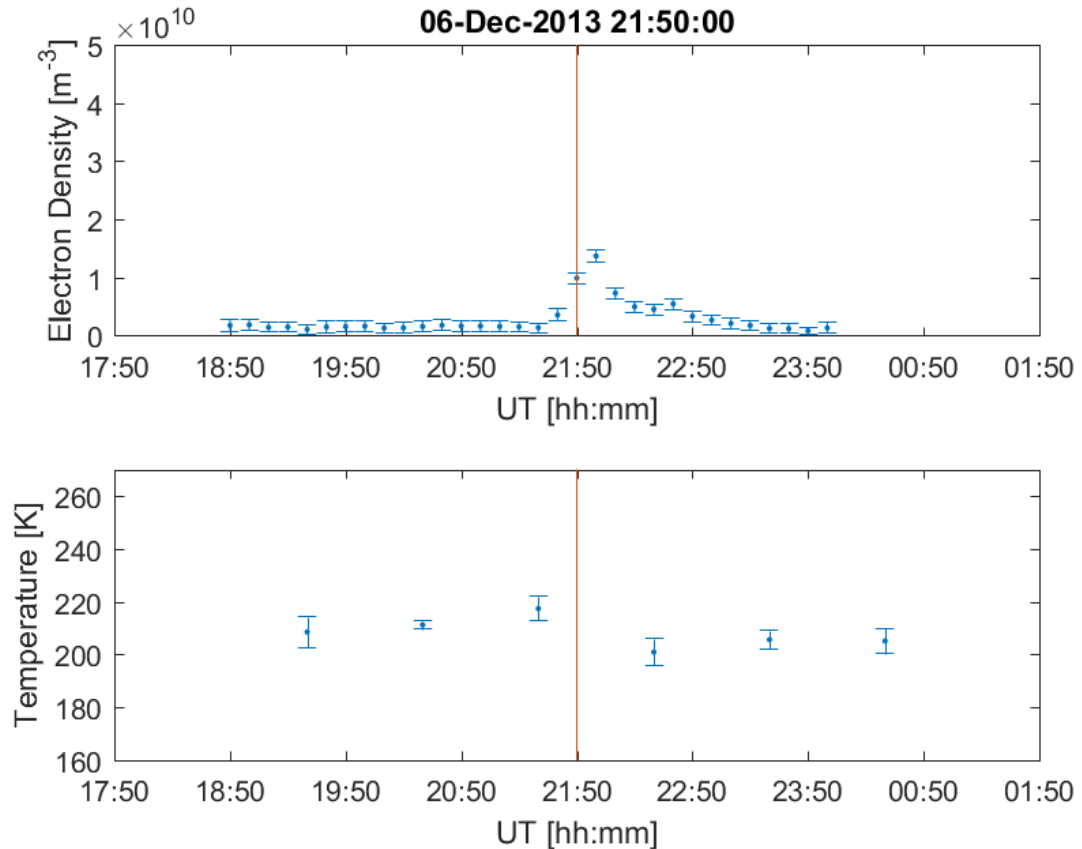


Figure 8.1.: This is an example plot with full coverage of the airglow data around the event. The electron density versus the time ± 3 h around the event is shown in panel 1, panel 2 shows the airglow variation in hourly resolution versus time. The vertical bars indicate the error. The time of the event is indicated by the red vertical line in both plots. The event is from the 6th of December 2013 at 21:50 UT. The radar experiment is *ipy*. The electron density is averaged over an altitude range of 87 - 90 km.

9. Results

9.1. Energetic Particle Precipitation Events

9.1.1. Events with Full Coverage of Temperature Data (Hourly Resolution)

The events with full coverage of temperature data in hourly resolution are listed in table 9.1. The criterion for a decreasing/ increasing electron density event is that the decrease/ increase has to be larger than the STD error bars. An event is stable, if the temperature change is within the errors of the estimate.

Event Time [UT]	T before	T after	decreasing or stable
2007/12/29 23:30:00	225 [K]	181 [K]	decreasing
2013/12/06 21:50:00	217 [K]	201 [K]	decreasing
2019/01/06 19:50:00	192 [K]	186 [K]	decreasing
2008/01/10 01:50:00	190 [K]	192 [K]	stable
2008/01/28 22:20:00	203 [K]	202 [K]	stable
2014/01/24 02:10:00	214 [K]	212 [K]	stable

Table 9.1.: Airglow temperature comparison before and after the events, the last column indicates whether the event is clearly decreasing or rather stable

Figure 9.1 and Figure 9.2 show the case plots for all the events covered by the temperature values with hourly resolution. Figure 9.1 shows the events with decreasing temperatures. The left column of plots shows the electron density versus altitude and time plots for indicated events. The first EPP event is commencing at 23:30 UT on 29th of December 2007 (top panel). The second EPP event is commencing at 21:50 UT on 6th of December 2013 (second panel). The third EPP event is commencing at 19:50 UT on 6th of January 2019 (third panel). The events are registered in the altitude range of 87-90 km. The right column shows the electron density versus time plots at an altitude range of 87-90 km and the temperature versus time plots. For the first event the electron density at the event starting time is $6.87 \times 10^9 [m^{-3}]$ (at 23:30 UT on 29th of December 2007). This event shows a rapid decrease of 44 K from 225 to 181 K, which recovers immediately and even increases in the data point after. An enhancement of the electron density can only be seen for about 30 min for this event. For the second event the electron density at the starting time is $9.92 \times 10^9 [m^{-3}]$ (21:50 UT on 6th of December 2013). The temperature drops 16 K from 217 to 201 K and then slowly increases over the next 2 hours. The density enhancement is visible for about 50 min. For the third event the electron density at the starting time is $9.05 \times 10^9 [m^{-3}]$ (19:50 UT on 6th of January

9. Results

2019). The temperature drops only 2 K from 214 to 212 K. The temperature then increases slowly over the next 2 temperature points for a few Kelvin. The density enhancement is about 40 min long.

9. Results

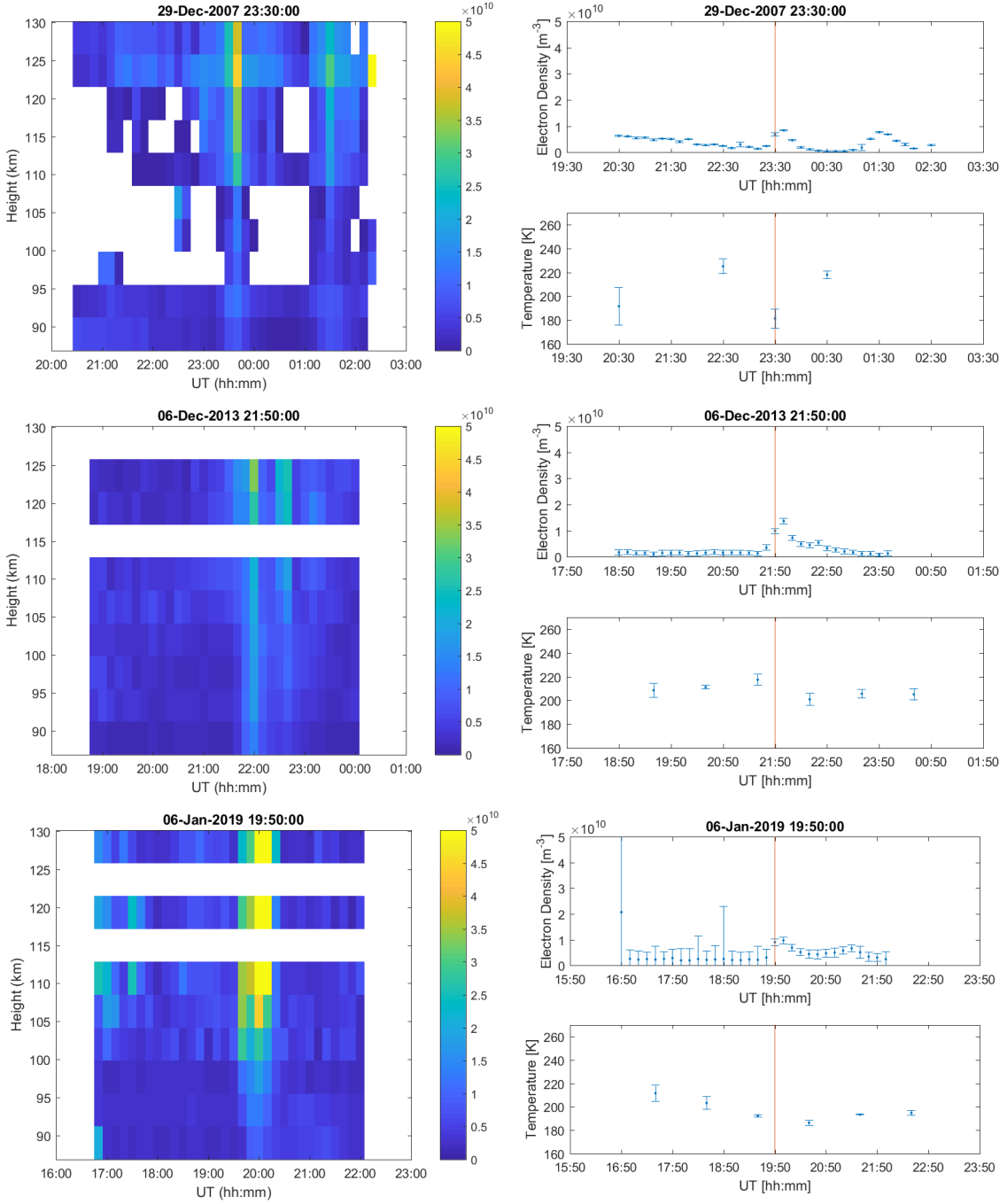


Figure 9.1.: This figure shows the events with decreasing temperatures. The left column of plots shows the electron density versus altitude and time plots for indicated events. The right column shows the electron density versus time plots at an altitude range of 87-90 km and the airglow temperature versus time plots.

9. Results

Figure 9.2 shows the events with stable temperatures. The left column of plots shows the electron density versus altitude and time plots for indicated events. The first EPP event is commencing at 01:50 UT on 10th of January 2007 (top panel). The second EPP event is commencing at 22:20 UT on 28th of January 2008 (second panel). The third EPP event is commencing at 02:10 UT on 24th of December 2014 (third panel). The events are registered in the altitude range of 87-90 km.

The right column shows the electron density versus time plots at an altitude range of 87-90 km and the temperature versus time plots. For the first event the electron density at the event starting time is $4.22 \times 10^9 [m^{-3}]$ (at 01:50 UT on 10th of January 2007). The electron density is enhanced for a couple of hours. For the second event the electron density at the starting time is $3.57 \times 10^{10} [m^{-3}]$ (at 22:20 UT on 28th of January 2008). The electron density at the event time is particularly high. The temperature drops in the hour after the event and increase slightly in the subsequent hour. For the third event the electron density at the starting time is $9.52 \times 10^9 [m^{-3}]$ (at 02:10 UT on 24th of December 2014). The temperature stays stable over about 2 hours past the event. The electron density enhancement varies for multiple hours.

9. Results

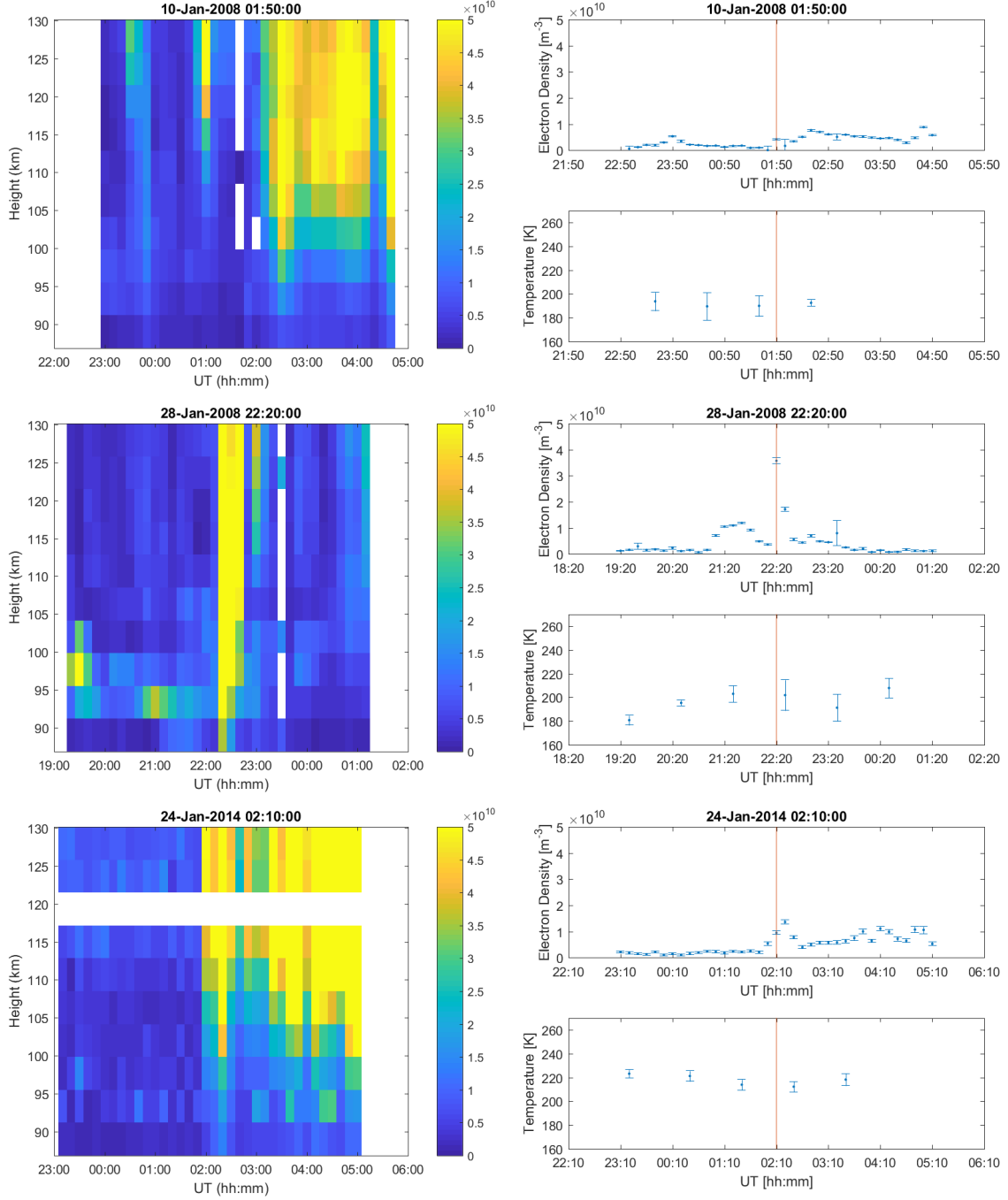


Figure 9.2.: This figure shows the events with stable temperatures. The left column of plots shows the electron density versus altitude and time plots for indicated events. The right column shows the electron density versus time plots at an altitude range of 87-90 km and the temperature versus time plots.

9. Results

For the scatter plots the temperature values from 1 hour before to 2 hours after the event are included. The electron density is averaged for the same hours and plotted on logarithmic scale. The codes for the scatter plot is found in Appendix A.2.4. The upper panel in Figure 9.3 shows the scatter plot for the events with decreasing temperature, see table 9.1. The scatter plot shows low neutral temperature values for high electron density values.

The superposed epoch plots include the temperature values in the ± 4 hour window of the event. The median, percentile 25 and percentile 75 is calculated for all the temperature points available from different events within the same epoch. These temperature points are then plotted versus the epochs A.2.5. The superposed epoch plot for the EPP events with decreasing temperature is shown in the lower panel of Figure 9.3. The decrease happens immediately at the event time. An hour later the temperature has recovered. Two hours past the event there is another short lived decrease, which is recovered 3 hours after the event and the temperature is increasing until epoch time 4. For the superposed epoch plot the percentiles 25 %, 50 % and 75 % of the airglow temperature data for each hour are calculated and plotted versus the time range of 4 hours before to 4 hours after the event, see A.2.5.

The detection had a threshold of increase by a factor of 5, here the whole range of densities is within $+/-5\%$ of the average.

The upper panel in Figure 9.4 shows the scatter plot of the events with stable temperature, the lower panel shows the superposed epoch plot. The scatter plot shows a rising temperature with EPP. The superposed epoch plot shows a small decrease in temperature at the event and a slight increase over the 2 following hours.

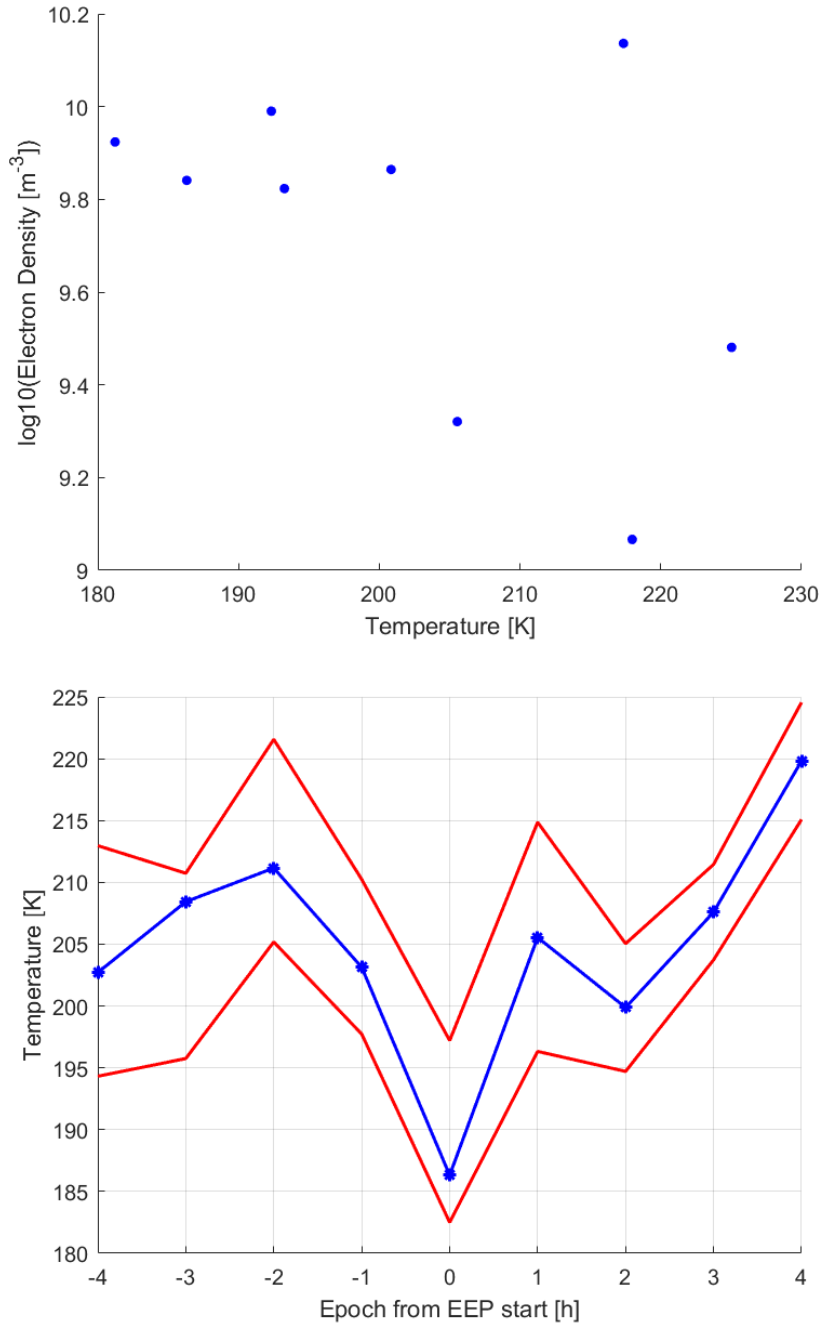


Figure 9.3.: This figure shows the events with decreasing temperatures. The upper panel shows scatter plot of the hourly averaged electron density versus the hourly airglow temperature. The lower panel shows the superposed epoch plot of the airglow temperature including percentiles 25 % (lower red line), 50 % (blue) and 75 % (upper red line) of the temperature. There are 2 - 4 values per temperature point.

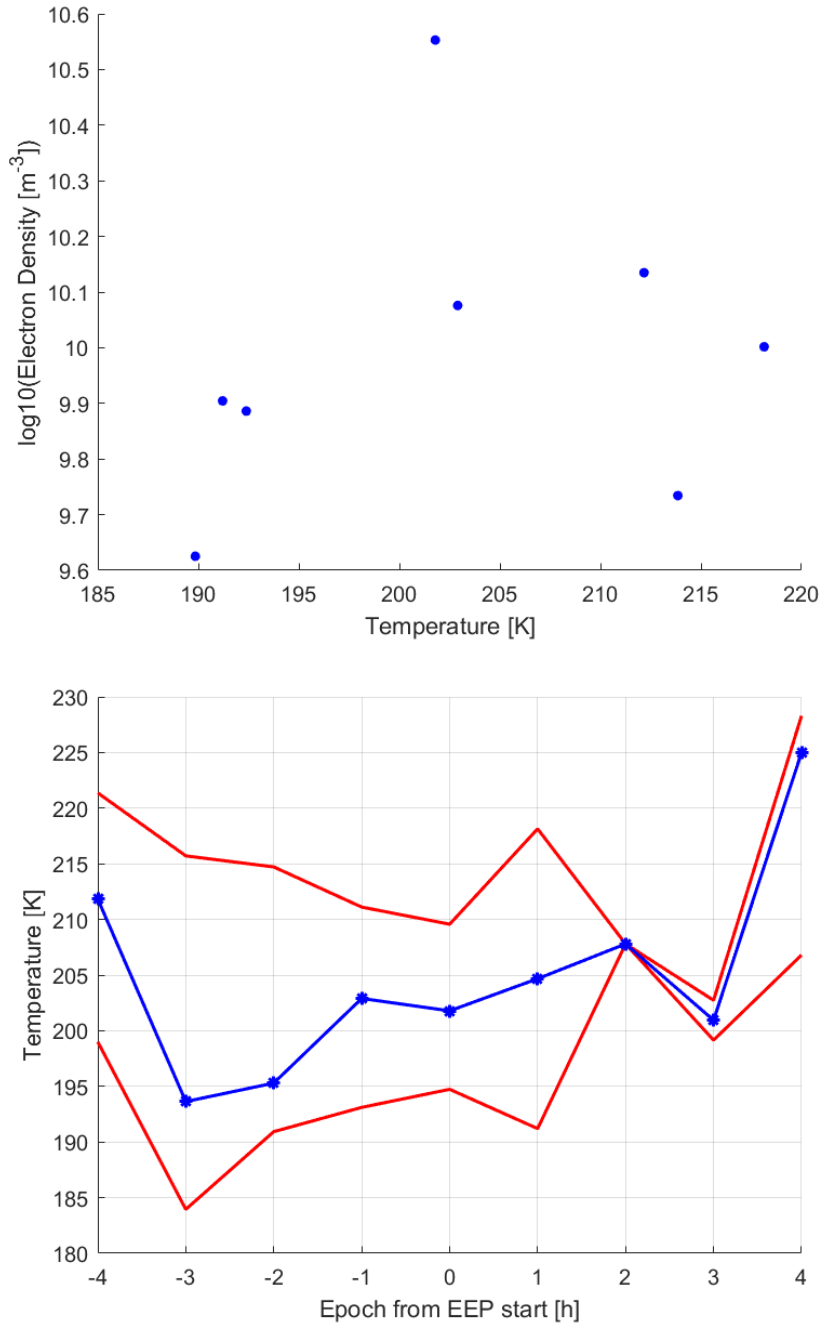


Figure 9.4.: This figure shows the events with stable temperatures. The upper panel shows scatter plot of the hourly averaged electron density versus the hourly airglow temperature. The lower panel shows the superposed epoch plot of the airglow temperature including percentiles 25 % (lower red line), 50 % (blue) and 75 % (upper red line) of the temperature. There are 2 - 3 values per temperature point, except at epoch 2 only 1 value is available.

9.1.2. Events with Partial Coverage of Temperature Data (Hourly Resolution)

Table 9.2 shows the list of event onsets for events, which are only partly covered by the hourly temperature points. Figure 9.5 shows the scatter plot and superposed epoch plot for listed events. The scatter plot shows an increasing response to EPP, so does the superposed epoch plot. The superposed epoch plot shows an increase in temperature at the event time lasting to the hour past the event. At epoch 2 a decrease is found, which is recovered at epoch 4.

EPP event onsets		
04-Dec-2007 03:30:00	08-Feb-2008 00:10:00	25-Jan-2014 02:40:00
18-Dec-2007 02:40:00	09-Feb-2008 22:20:00	28-Jan-2014 19:10:00
30-Dec-2007 01:20:00	04-Feb-2011 04:50:00	05-Feb-2016 19:40:00
03-Jan-2008 22:00:00	07-Feb-2011 22:50:00	06-Feb-2016 19:50:00
09-Jan-2008 00:50:00	01-Dec-2011 20:10:00	06-Feb-2016 23:50:00
10-Jan-2008 21:30:00	16-Jan-2012 20:30:00	08-Feb-2016 02:20:00
11-Jan-2008 00:20:00	17-Jan-2012 00:50:00	15-Jan-2017 14:30:00
13-Jan-2008 21:50:00	23-Jan-2014 06:50:00	02-Feb-2017 16:40:00
19-Jan-2008 23:50:00	23-Jan-2014 14:00:00	02-Feb-2017 19:20:00
29-Jan-2008 13:30:00	24-Jan-2014 15:20:00	05-Jan-2019 21:50:00

Table 9.2.: EPP event onsets found, which are partly covered by the hourly airglow temperature

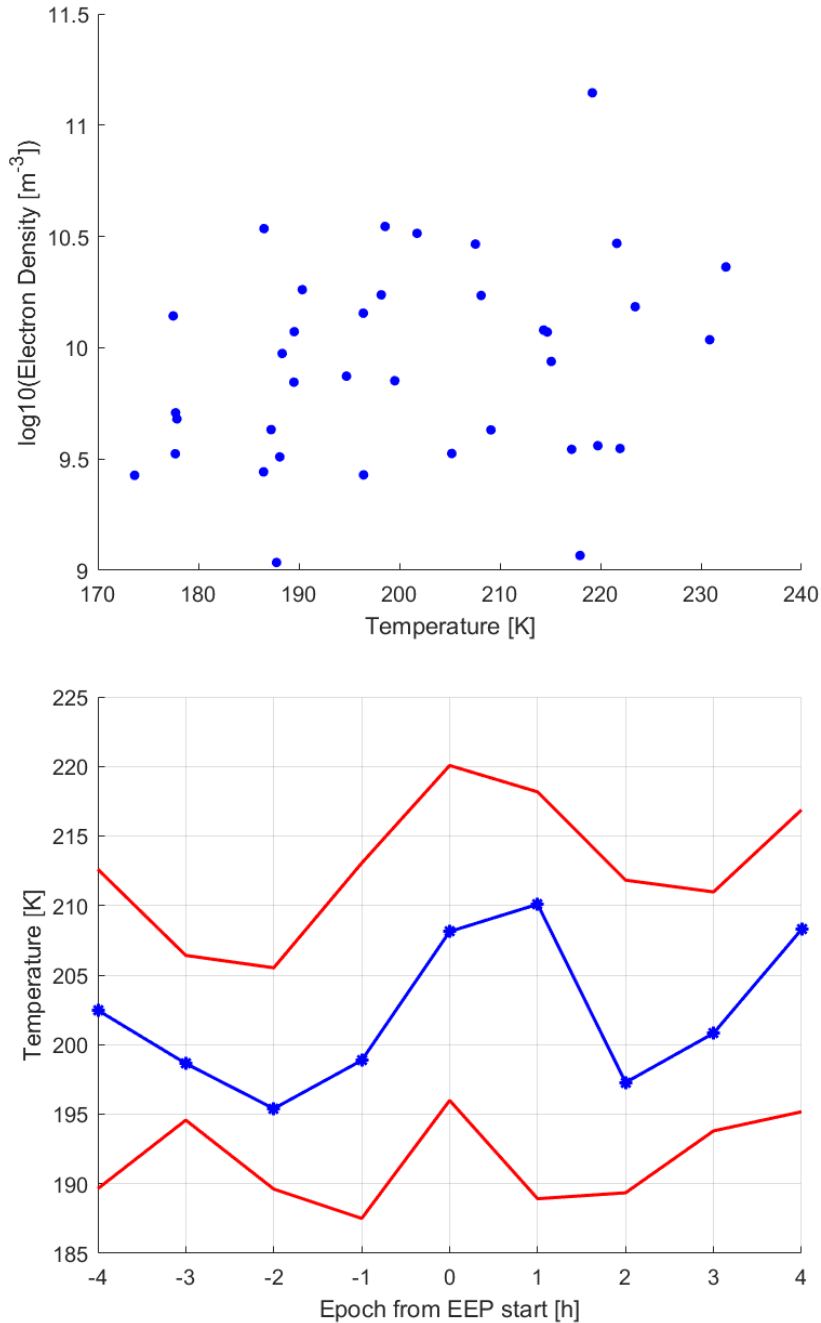


Figure 9.5.: This figure shows the events with gaps in the hourly temperature values. The upper panel shows scatter plot of the hourly averaged electron density versus the hourly airglow temperature. The lower panel shows the superposed epoch plot of the airglow temperature including percentiles 25 % (lower red line), 50 % (blue) and 75 % (upper red line) of the temperature. There are in between 13 -19 values per temperature point.

9.1.3. Events with Full Coverage of Temperature Data (Half-Hourly Resolution)

The events with full coverage of temperature data in half-hourly resolution are listed in table 9.3. Comparing this to Table 9.1, event 2013/12/06 21:50:00 and event 2007/12/29 23:30:00 are covered by both hourly and half-hourly temperature data and is classified as decreasing both times. Event 2014/01/24 02:10:00 is also covered by hourly and half-hourly temperature data, but is classified as stable in the hourly and increasing in the half-hourly temperature data. The criterion for a decreasing/ increasing electron density event is that the decrease/ increase has to be larger the STD error bars. An event is stable, if the error bars clearly overlap.

Event Time [UT]	T before	T after	decreasing or increasing
2007/12/29 23:30:00	234 [K]	179 [K]	decreasing
2011/02/07 22:50:00	205 [K]	187 [K]	decreasing
2013/12/06 21:50:00	210 [K]	196 [K]	decreasing
2014/01/25 02:40:00	221 [K]	210 [K]	decreasing
2014/01/24 02:10:00	198 [K]	220 [K]	increasing
2014/01/24 15:20:00	217 [K]	222 [K]	stable

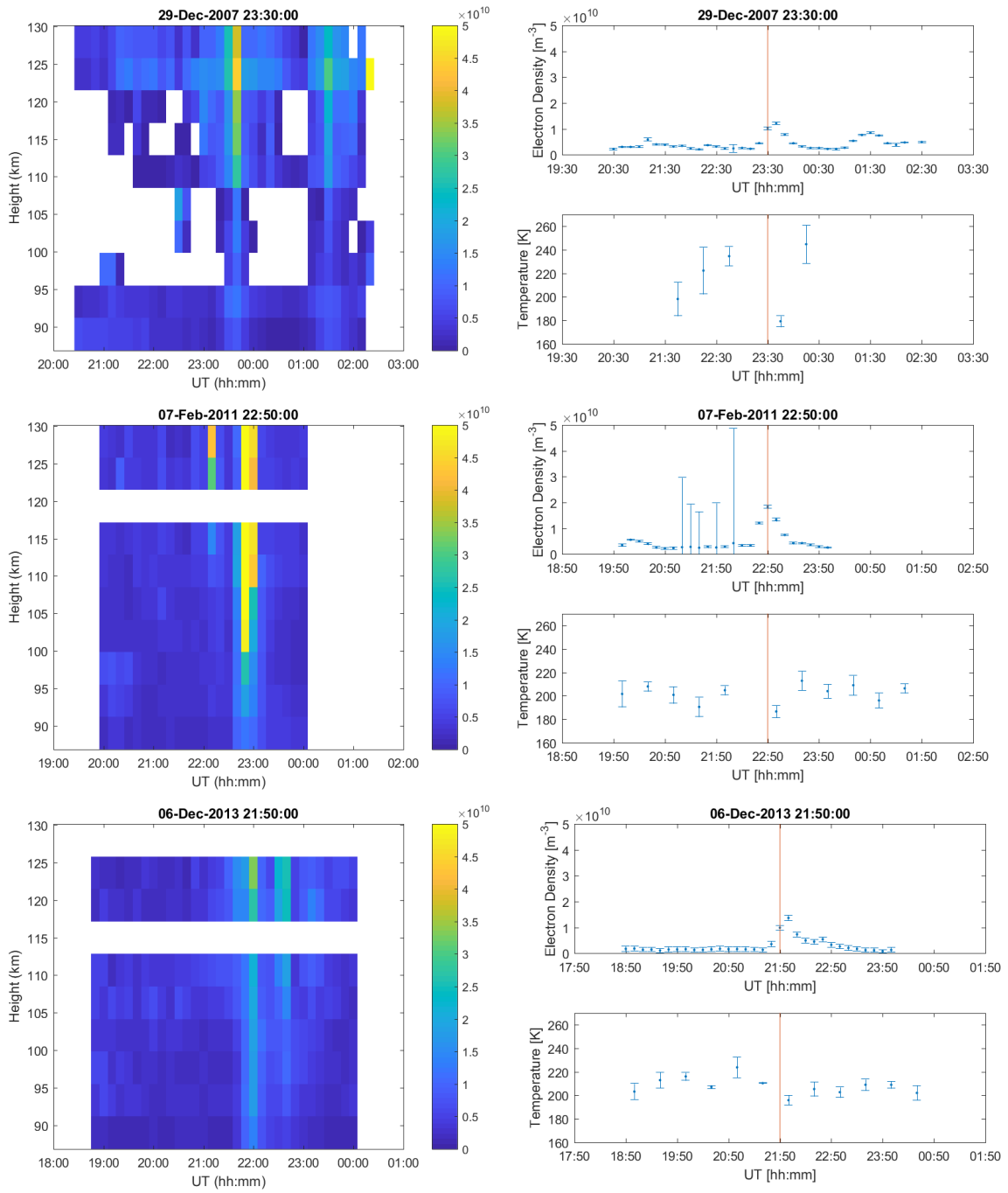
Table 9.3.: Airglow temperature comparison before and after the events, the last column indicates whether the event is clearly decreasing or rather stable

Figure 9.5 and Figure 9.6 show the case plots for all the events covered by the temperature values with hourly resolution. Figure 9.5 shows the events with decreasing temperatures. The left column of plots shows the electron density versus altitude and time plots for indicated events. The first EPP event is commencing at 23:30 UT on 29th of December 2007 (top panel), the event is registered in the altitude range of 91-94 km. The second EPP event is commencing at 22:50 UT on 7th of February 2011 (second panel), the event is registered in the altitude range of 91- 94 km. The third EPP event is commencing at 21:50 UT on 6th of December 2013 (third panel), the event is registered in the altitude range of 87-90 km. The forth EPP event is commencing at 02:40 UT on 25th of January 2014 (forth panel), the event is registered in the altitude range of 87-90 km. The right column shows the electron density versus time plots at the altitude range the event is detected and the temperature versus time plots. For the first event the electron density at the event starting time is $1.02 \times 10^{10} [m^{-3}]$ (at 23:30 UT on 29th of December 2007). The temperature increases for 55 K from 234 to 179 K to then recover again in the next half-hour. The event is lasting for about 30 min. For the second event the electron density at the starting time is $1.84 \times 10^{10} [m^{-3}]$ (at 22:50 UT on 7th of February 2011). The decrease is 18 K from 205 to 187 K and followed by an increase and a fairly stable temperature in the following hours. The electron density enhancement lasts for about 40 min. For the third event the electron density at the starting time is $9.92 \times 10^9 [m^{-3}]$ (at 21:50 UT on 6th of December 2013). The temperature initially decreases for 14 K from 210 to 196 K to then slightly increase and stay about stable over the next hours. The electron density enhancement is longer lived and lasts about 70 min. For the forth event the electron density at the starting time is $9.52 \times 10^9 [m^{-3}]$ (at 02:40 UT on 25th of January 2014). The temperature drops from

9. Results

221 to 210 K and then stays stable. The EPP lasts for hours after the event.

9. Results



9. Results

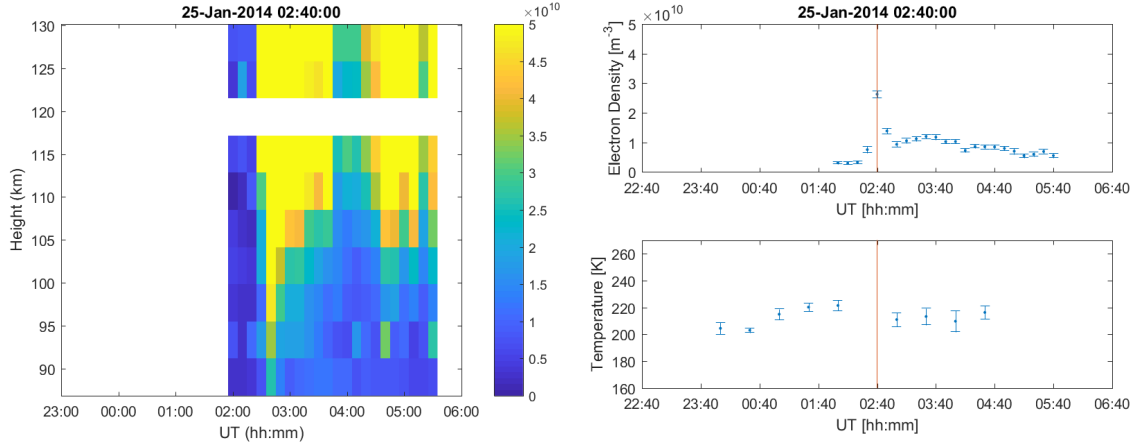


Figure 9.5.: This figure shows the events with decreasing temperatures. The left column of plots shows the electron density versus altitude and time plots for indicated events. The right column shows the electron density versus time plots at an altitude range of 91-94 km (1st and 2nd plot) and 87-90 km (3rd and 4th plot) and the temperature versus time plots.

Figure 9.6 shows the event with stable temperature and the event with increasing temperature. The left column of plots shows the electron density versus altitude and time plots for indicated events. The first EPP event is commencing at 15:20 UT on 24th of January 2014 (top panel). The second EPP event is commencing at 02:10 UT on 24th of January 2014 (second panel). The events are registered in the altitude range of 87-90 km. The right column shows the electron density versus time plots at an altitude range of 87-90 km and the temperature versus time plots. For the first event the electron density at the event starting time is $1.53 \times 10^{10} [m^{-3}]$ (at 15:20 UT on 24th of January 2014). The electron density stays stable for the following hours. The event is short lived for about only 10 min. For the second event the electron density at the starting time is $2.63 \times 10^{10} [m^{-3}]$ (at 02:10 UT on 24th of January 2014). The temperature increases from 198 K to 220 K in the following 30 min and then drops to about its value before the event. The EPP event lasts for several hours.

9. Results

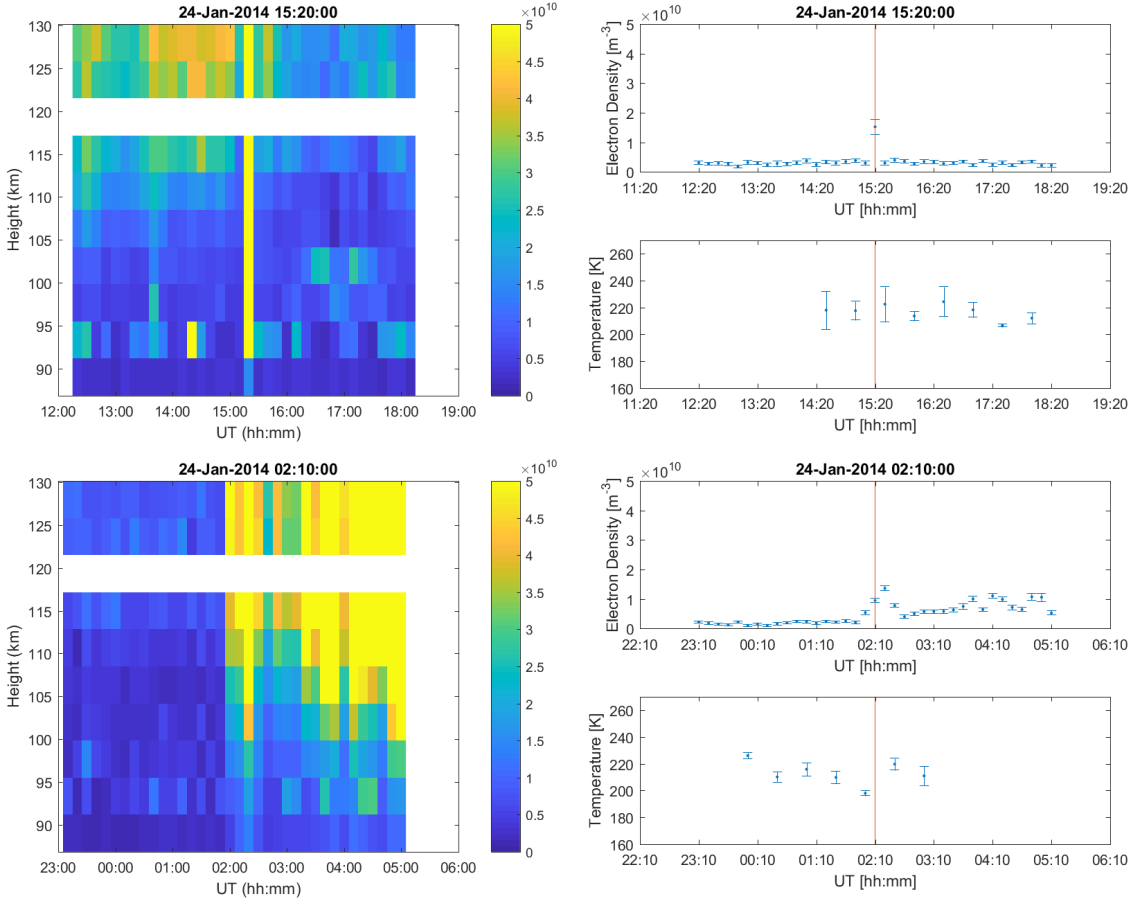


Figure 9.6.: This figure shows the events with decreasing temperatures. The left column of plots shows the electron density versus altitude and time plots for indicated events. The right column shows the electron density versus time plots at an altitude range of 87-90 km and the temperature versus time plots.

9. Results

The upper panel in Figure 9.7 shows the scatter plot for the events with decreasing temperature, see table 9.1. A negative response of EPP to the temperature is found in the scatter plot. The superposed epoch plot for the EPP events with decreasing temperature is shown in the lower panel of Figure 9.7. A sharp decrease in temperature is found at the event time, which is immediately recovered half an hour later. Until epoch 3 the temperature decreases.

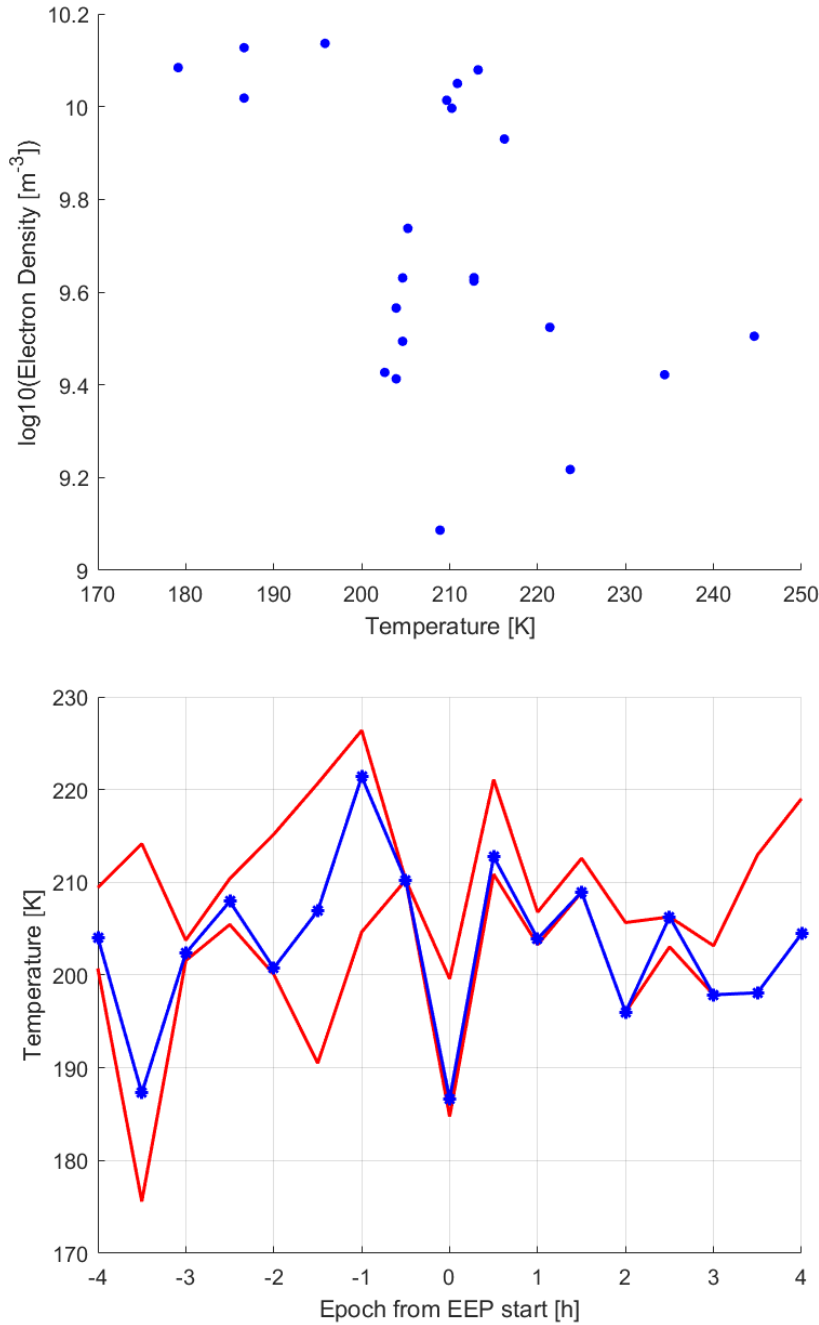


Figure 9.7.: This figure shows the events with decreasing temperatures. The upper panel shows scatter plot of the half-hourly averaged electron density versus the half-hourly airglow temperature. The lower panel shows the superposed epoch plot of the airglow temperature including percentiles 25 % (lower red line), 50 % (blue) and 75 % (upper red line) of the temperature. The temperature points include 3 to 5 values, except 0.5 hour before the event only includes 1 value.

9.1.4. Events with Partial Coverage of Temperature Data (Half-Hourly Resolution)

The list of EPP event onsets with partly coverage of the temperature data in half-hourly resolution is found in Table 9.4. The scatter plot and the superposed epoch plot for this group is shown in Figure 9.8. No coherent behaviour can be found in the scatter of these data. The superposed epoch plot shows an increase of temperature at the event time, a drop 30 min later followed by a gradual increase over 30 min until another drop of temperature at epoch 3.

EPP event onsets		
18-Dec-2007 02:40:00	13-Feb-2008 04:00:00	06-Feb-2016 19:50:00
30-Dec-2007 01:20:00	04-Feb-2011 06:20:00	06-Feb-2016 23:50:00
02-Jan-2008 00:00:00	04-Feb-2011 18:50:00	08-Feb-2016 02:20:00
03-Jan-2008 22:00:00	01-Dec-2011 20:10:00	02-Feb-2017 16:40:00
10-Jan-2008 21:30:00	16-Jan-2012 20:30:00	02-Feb-2017 19:20:00
11-Jan-2008 00:20:00	17-Jan-2012 00:50:00	08-Jan-2018 07:20:00
28-Jan-2008 22:20:00	23-Jan-2014 14:00:00	05-Jan-2019 21:50:00
09-Feb-2008 22:20:00	28-Jan-2014 19:10:00	06-Feb-2019 06:20:00
12-Feb-2008 20:20:00	05-Feb-2016 19:40:00	

Table 9.4.: EPP event onsets found, which are partly covered by the half-hourly airglow temperature

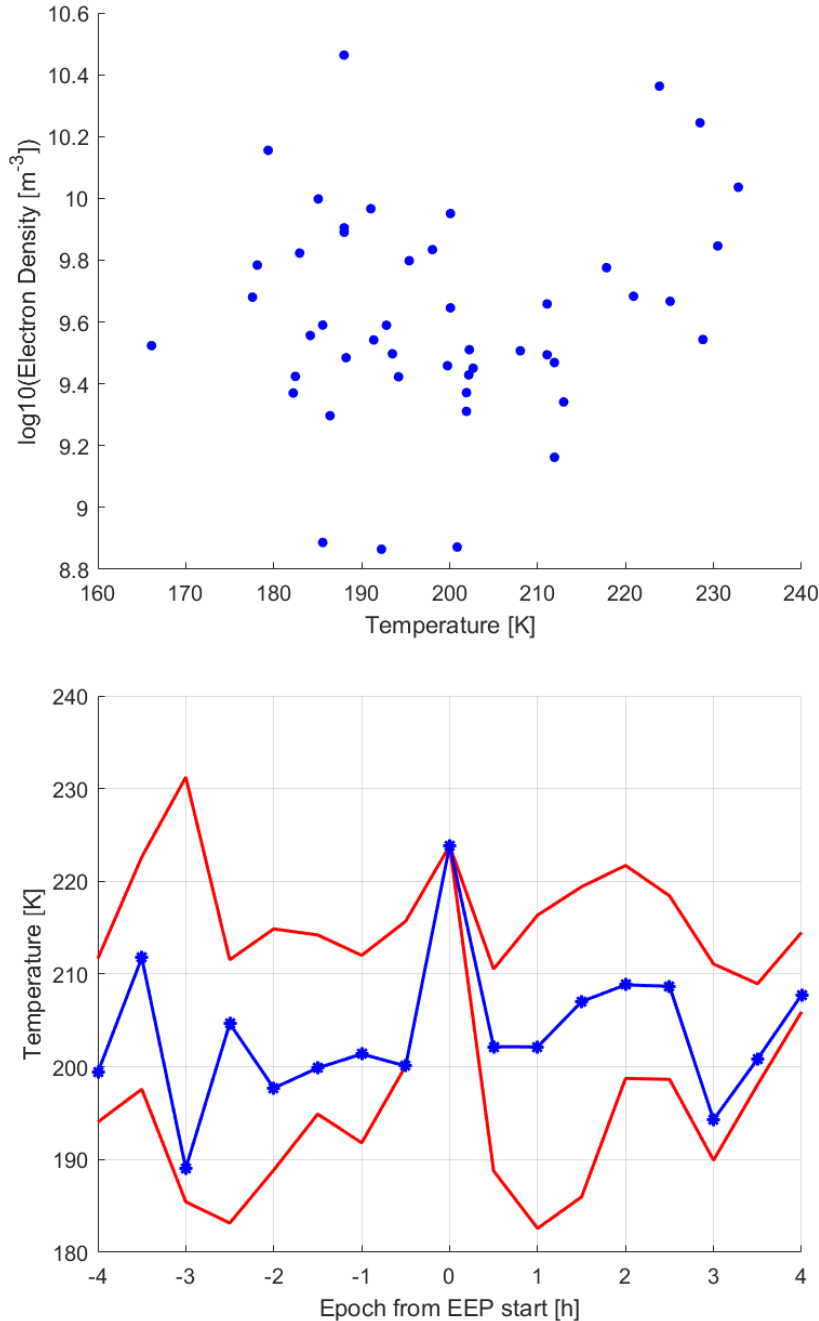


Figure 9.8.: The upper panel shows scatter plot of the half-hourly averaged electron density versus the half-hourly airglow temperature. The lower panel shows the superposed epoch plot of the airglow temperature including percentiles 25 % (lower red line), 50 % (blue) and 75 % (upper red line) of the temperature. There are 15-16 values per temperature point from -4 to -1 hour before the event. At 0.5 hours before the event only 3 values and at the event only 1 value is available. From +0.5 hour to +4 hours there are 7-16 values per temperature point.

9.2. Sporadic E-layers

9.2.1. Events with Full Coverage of Temperature Data (Hourly Resolution)

Searching for EPP onsets led to find sporadic E-layers in the radar data (onset times shown in table 9.5). The plots for the sporadic E-layers are found in Appendix A.3. An example is given in Figure 9.9. The event of 17:20 UT on the 26th of January 2008 shows a short lived electron density enhancement in the altitude range of 87-90 km. There is an initial temperature drop at the event start followed by an increase for the next 2 hours. The scatter plot and the superposed epoch plot for sporadic E-layer is shown in Figure 9.10. The scatter plot shows no coherent behaviour. The superposed epoch plot shows a slow dropping of temperature from epoch -1 to epoch +2 and an increase until epoch 3.

sporadic E-layers event onsets		
26-Jan-2008 17:20:00	29-Jan-2008 22:50:00	15-Jan-2017 15:50:00
28-Jan-2008 19:30:00	30-Jan-2008 19:40:00	12-Feb-2019 21:40:00
28-Jan-2008 21:10:00	31-Jan-2008 05:30:00	13-Feb-2019 18:00:00

Table 9.5.: EPP event onsets found, which are partly covered by the half-hourly airglow temperature

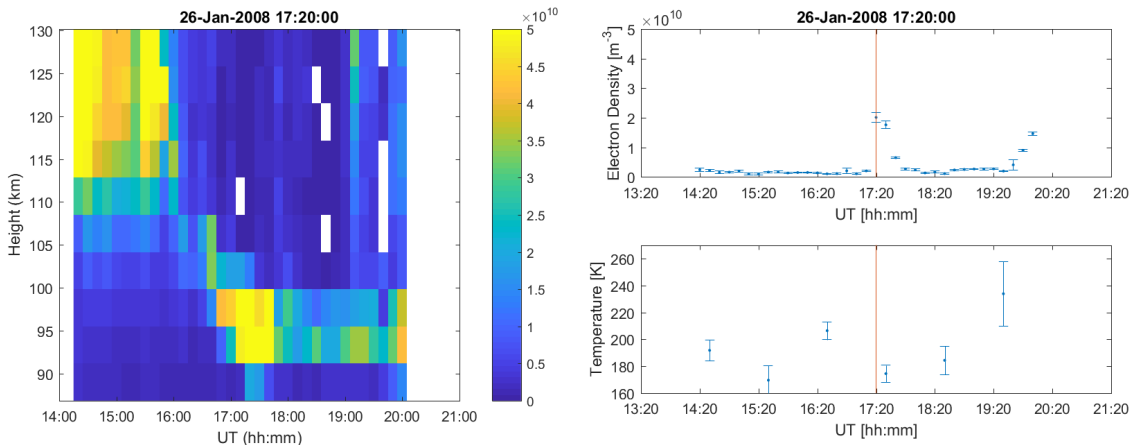


Figure 9.9.: This figure shows one example of a sporadic E-layer. The onset of the sporadic E-layer is detected at 17:20 UT on the 26th of January 2008 in the altitude range of 87-90 km. The left plot shows the electron density versus altitude and time plots for indicated events. The right plot the electron density versus time plots at an altitude range of 87-90 km and the neutral temperature versus time plots.

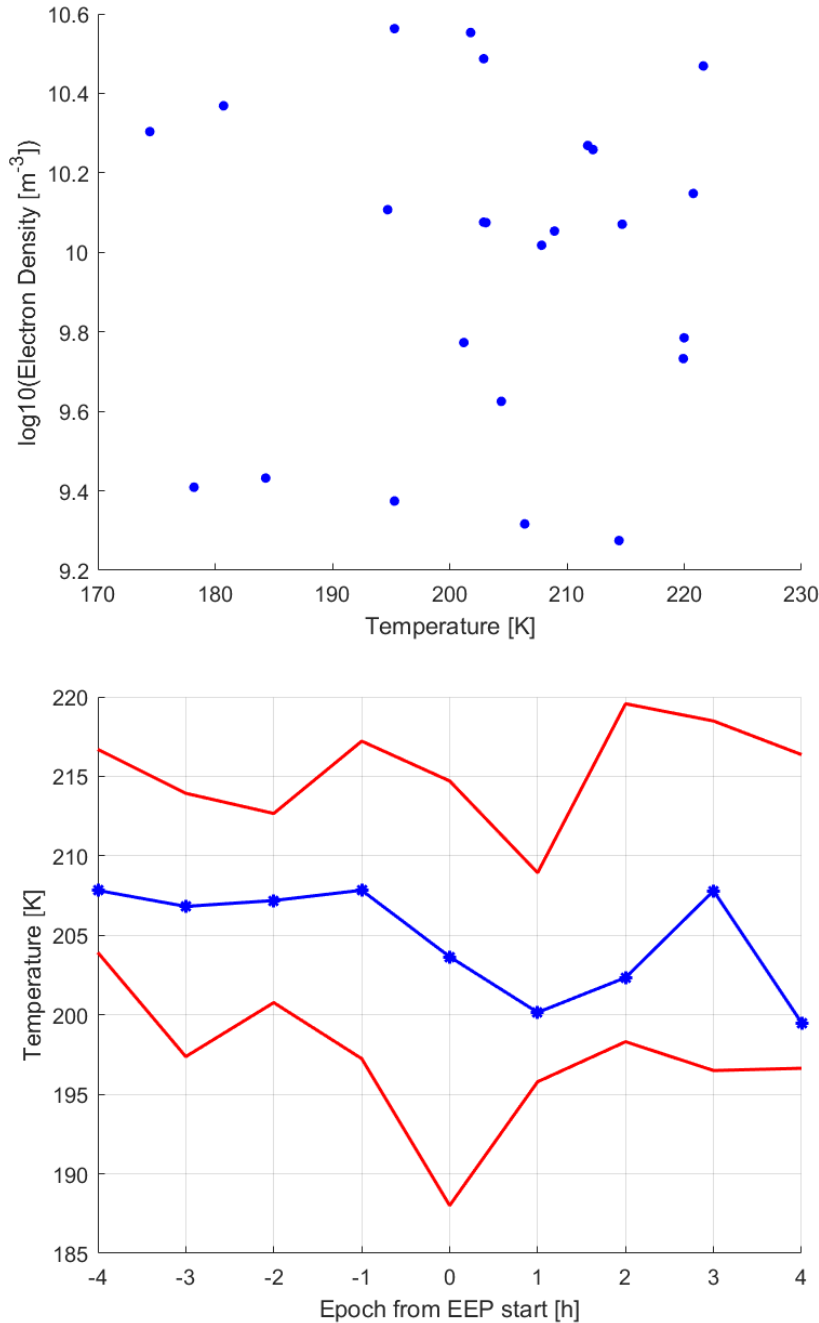


Figure 9.10.: This figure shows the scatter plot of the sporadic E-layer events. The upper panel shows scatter plot of the hourly averaged electron density versus the hourly airglow temperature. The lower panel shows the superposed epoch plot of the airglow temperature including percentiles 25 % (lower red line), 50 % (blue) and 75 % (upper red line) of the temperature. There are in between 7 - 10 values per temperature point.

9.2.2. Events with Partial Coverage of Temperature Data (Hourly Resolution)

The 13 partly covered sporadic E-layer events are combined for a scatter plot and a superposed epoch plot, see Figure 9.11. The scatter plot shows a clear positive response of the EPP on the mesopause temperature. The superpose epoch plot also shows an increase at the time of the event and an decrease at the hour after.

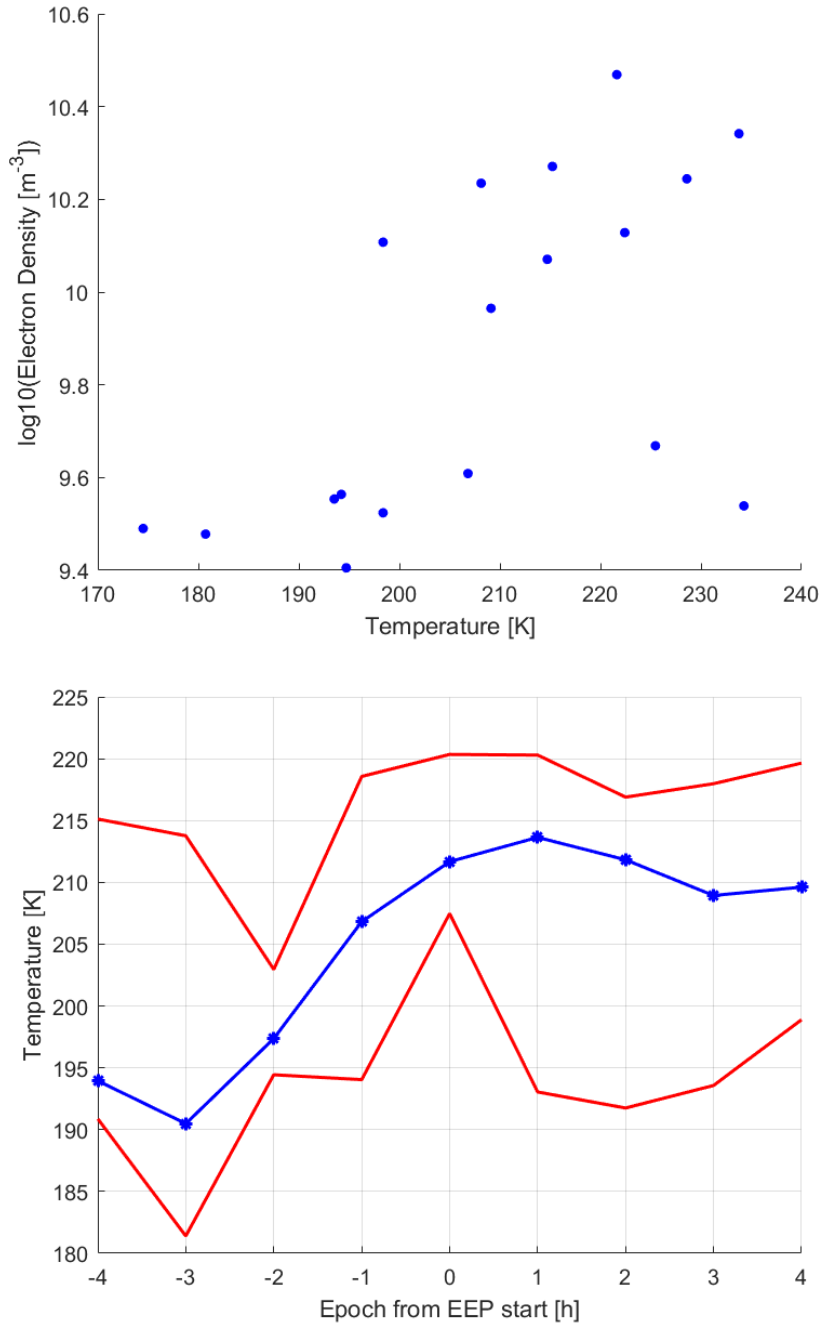


Figure 9.11.: This figure shows the scatter plot of the sporadic E-layer events. The upper panel shows scatter plot of the hourly averaged electron density versus the hourly airglow temperature. The lower panel shows the superposed epoch plot of the airglow temperature including percentiles 25 % (lower red line), 50 % (blue) and 75 % (upper red line) of the temperature. There are in between 4 - 9 values per temperature point.

10. Discussion

10.1. Discussion on EPP Effects on the Mesopause Temperature

In total six events covered by hourly temperature values are found and six event covered by half-hourly temperature. Three of these events are found in both sets. The general temperature variation of the half-hourly temperature during the season 2018/19 is shown in Figure 10.1.

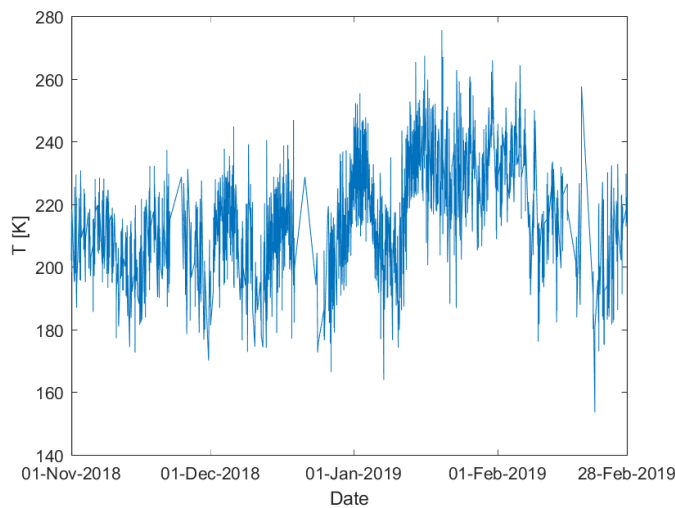


Figure 10.1.: Airglow temperature variations of the winter season 2018/2019

Table 9.1 shows that the events covered by hourly temperature values show an average decrease of 22 K in the hour of the EPP event. Table 9.3 shows an average decrease of 24.5 K for cases covered by half-hourly temperature values within 0.5 hours of the event. The pre-EPP level (temperature within 1 hour before the event) varied between 192 to 225 K for the hourly temperature value covered events and between 205 to 234 K for the half-hourly temperature value covered events. The temperature decreased to the range of 181-201 K for the hourly temperature value covered events and to the range of 179-210 K for the half-hourly temperature value covered events at the EPP onset of the events.

Inspecting the scatter plots for events with an immediate decrease in temperature at the onset for hourly and half-hourly temperature value covered data (Figure 9.3 and Figure 9.7), a decrease of temperature with increasing electron density can be seen. The superposed epoch plots, Figure 9.3 and Figure 9.7, of the same events both show a steep decrease in temperature

10. Discussion

at the zero epoch time and a quick recovery and even increase over the pre-EPP level in the next data point. In Figure 9.1 the event at 23:30 UT on 29th of December 2007 shows an electron density enhancement before the event onset, which could be why the temperature seems to be low level 3 hours before the event. The temperature right before the event is high level again as the electron density is low for about 1.5 hours before the event. This is a typical example, which shows how temperature and electron density anti-correlate and thus produce the negatively sloping scatter plot. The data for the scatter plot is taken 1 hour before to 2 hours after the onset, so any previous electron density enhancement is not included. The other two events in the same Figure clearly show only one event onset within the 6-hour window around the event.

Inspecting the half-hourly temperature covered EPP events, in Figure 9.2 the event at 01:50 UT on 10th of January 2007 shows a density enhancement 2 hours before the event time, and even another enhancement higher up, less than an hour before the event which might affect the response. The temperature points at the electron density enhancement before seem to lower the temperature, but the error bars of the temperature points at this place are overlapping. Both the event at 01:50 UT on 10th of January 2007 and the event at 02:10 UT on 24th of January 2014 are onsets for longer lasting events (several hours), which explains very small temperature variations during the events. The latter event does show a decrease in temperature, when comparing to the level of 2 hours before the event. The averaging is regularly spaced in time so that the event onset can fall into the beginning or the end of the averaging window. Thus, an EPP onset taking place at the end of the temperature averaging hour can result in a smoother temperature decrease. The event at 22:20 UT on 28th of January 2008 shows a sporadic E-layer enhancement before the EPP event. The temperature is increasing before this event and seems to slightly drop an hour past the event. The increase could be explained by the sporadic E-layer, as the superposed epoch for sporadic E-layers suggests a gently increasing temperature. The decrease has a relatively big error bar, but could be explained by the EPP event.

The behaviour of the events with a stable temperature covered by hourly averages is shown scatter plot in Figure 9.4. The temperatures are staying between 190 to 214 K and are more comparable to the decreased level of the decreasing cases. The plot does show a stable temperature response to the EPP, but suggests a slight increase after the event in temperature. The superposed epoch plot shows a drop in temperature at the event time and the slight increase in temperature in the hours after, as seen in the scatter plot.

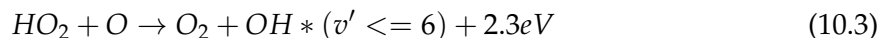
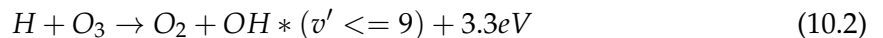
Only one event with stable temperature is found in half-hourly temperature data and is shown in Figure 9.6. This event shows a very short enhancement for only 10 min. In addition a variation in electron density, which could be a sporadic E-layer, is found at 91-94 km height before and after the event. The short event time and the variations of the electron density in 91-94 km height could explain the quite stable temperature values. The error bars are overlapping, nonetheless the electron density seems to decrease 0.5 hours past the event, then recover to decrease again about 2 hours later.

Additionally, one event with increasing temperature was found in half-hourly temperature data at 02:10 UT on 24th of January 2014, see Figure 9.6. The temperature clearly decreases

from 1 hour before to half an hour before. Due to the averaging the data value before the event might include the immediate effect of the event and the point after could include the increase, which is also observed in the other events classified as decreasing events. The decrease from the temperature point at 01:30 UT (210 K) to the point at 02:00 UT (198 K) is 12 K. The EPP, in this case, lasts for several hours. The same event is covered by hourly temperature data and sorted into the category stable, showing only the mentioned decrease in the data point before the event. The increase is not visible in the data point after the event but in the data point about 1.5 hours past the event.

Looking at the scatter plots for hourly and half-hourly temperature values partly covering the event, Figure 9.5 and Figure 9.8, different responses of the temperature to the EPP are mixed. The superposed epoch plots show an increase at the event hour which drops after 1-2 hours. The sharp decrease at the time of the event could be missing, as too many different behaviours are being mixed in the plot or as there are not enough temperature points available in the immediate time around the event, which is why they were classified in the partly covered by temperature data in the first place.

We found that the mesopause temperature responds with a decrease or stays stable at EPP. The temperature decrease may mean that the EPP ionisation changes the mesosphere chemical composition decreasing the population of excited OH at the top of the layer. As a consequence, the airglow peak height changes and the temperatures are probed at lower altitudes. The possibility of a change in the height distribution of the OH airglow emission during auroral events is also discussed in Suzuki et al. (2010). This is because electron impacts dissociate oxygen molecules and change the chemical composition of the atmosphere [25]. Thus, less O₃ is produced which is needed to produce rotational OH molecules 10.1. The dissociation of O₂ by energetic electrons therefore leads to a decrease in the production rate of OH molecules, see equation 10.1 and equation 10.2 or equation 10.3 during polar night [20].



When the rotational OH intensity profile is fitted, at the peak height of the layer the corresponding temperature value is found. The peak is assumed at the wrong height (further down), when the intensity layer shrinks from above into an asymmetric shape, due to EPP and OH* decrease. The temperature profile from the SABER satellite, shown Figure 10.2, shows the variation of the temperature with the altitude. When the intensity peak of the OH rotational molecules changes, the temperature values are increased or decreased depending on the gradient of the temperature profile at a particular height and time.

Excluding the decreased value at the EPP onset, the values of temperatures from the point before the event to the first increasing point past the event (about 1 hours after the event) are given in table 10.1 for hourly temperature data and in table 10.2 for half-hourly temperature. The average increase for increasing events is 6 K. The average decrease for decreasing events is 8 K. The effect of EPP on the mesopause temperature could be less visible after 1 h past the

event, that is why the increase could already be over in cases of EPPs with a short duration (few minutes). An increase in temperature could be explained by particle heating. Particle heating is produced by particles of the EPP colliding with the ones in the neutral atmosphere. This heating process is depending on the incident particles energy and enough energy flux depositions in the right altitudes [7].

Event Time [UT]	T pre-EPP level	T increase	decreasing / increasing
2007/12/29 23:30:00	225 [K]	218 [K]	decreasing
2008/01/28 22:20:00	203 [K]	208 [K]	increasing
2013/12/06 21:50:00	217 [K]	206 [K]	decreasing
2014/01/24 02:10:00	214 [K]	218 [K]	increasing
2019/01/06 19:50:00	192 [K]	193 [K]	increasing
2008/01/10 01:50:00	190 [K]	no data	no data

Table 10.1.: Table of events covered by hourly temperature values

Event Time [UT]	T pre-EPP level	T increase	decreasing / increasing
2007/12/29 23:30:00	234 [K]	244 [K]	increasing
2011/02/07 22:50:00	205 [K]	213 [K]	increasing
2014/01/24 02:10:00	210 [K]	220 [K]	increasing
2013/12/06 21:50:00	210 [K]	205 [K]	decreasing
2014/01/25 02:40:00	221 [K]	213 [K]	decreasing
2014/01/24 15:20:00	217 [K]	222 [K]	stable

Table 10.2.: Table of events covered by half-hourly temperature values

10.2. Discussion on Sporadic E-layer Effects on the Mesopause Temperature

The superposed epoch plot for the events covered by hourly temperature data in Figure 9.10, shows a decrease in temperature at the event time followed by a slow increase an hour later. The behaviour at the event onset is similar to the EPP-caused temperature response for the events fully covered by temperature data. The superposed epoch plot for the events partly covered by hourly temperature data, Figure 9.11, shows an increase in temperature starting at epoch -1 before the event lasting to hour 3 past the event. This could be due to the lacking points in the immediate timespan around the event, which could have shown an immediate temperature decrease. Again the behaviour at the event onset is similar to the EPP response for the events only partly covered by temperature data. The scatter plots in Figure 9.10 and Figure 9.11 show positive response of the temperature to EPP. The onsets of sporadic E-layers are harder to determine than for EPP, as the onsets seem more gradual.

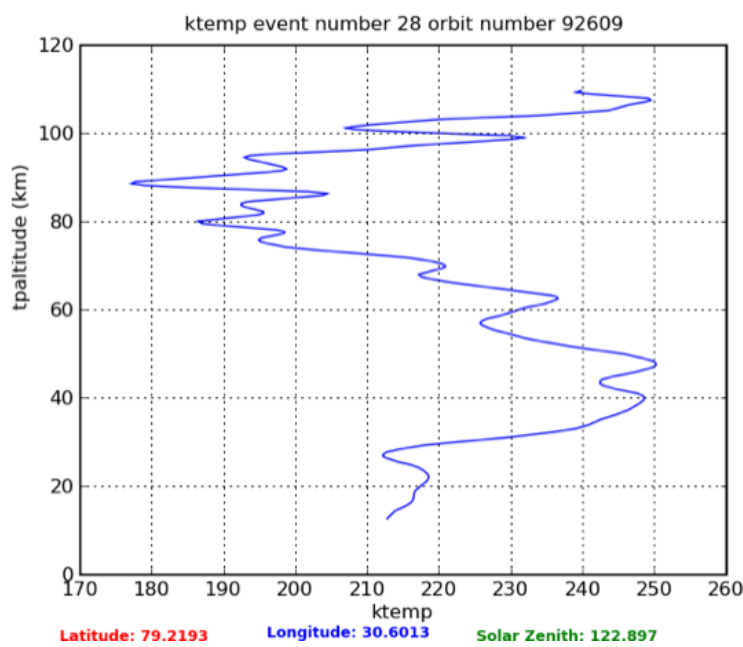


Figure 10.2.: Limb sounding of the SABER (sounding of the atmosphere using broadband emission radiometry) satellite at 22:57 UT on 6th of January 2019 close to Svalbard [26].

11. Conclusion and Outlook

A total of 10220 hours of electron density measurements and corresponding airglow measurements are analysed in this thesis. Nine different events of electron density enhancements covered by simultaneously measured mesopause temperatures are found. They are analysed to investigate if there is any coherent behaviour between the electron precipitation, which reaches the D-region, and the mesopause temperature.

The response of EPP on the mesopause temperature is predominately a decrease in an order of magnitude 20 K, which recovers within the next 0-5 hour-1 hour. The average rise of temperatures from the background level to the first increase of temperature within 2 hours past the event is 7 K. The temperature decrease may mean that the EPP ionisation changes the mesosphere chemical composition decreasing the population of excited OH at the top of the layer. As a consequence, the airglow peak height changes and the temperatures are probed at lower altitudes. The irradiance of the airglow is investigated for finding out if the change in the OH rotational molecules intensity decreased the temperature during the events. The increase in temperature after the drop for continuing precipitation could be explained by particle heating.

The response of sporadic E-layers on the mesopause temperature at the onset is comparable to the ones for EPP, even though the decrease in temperature is smaller than for EPP. After the initial decrease, no subsequent decrease is found for sporadic E-layers, the temperature rises slowly for about 2-3 hours after the event. This could depend on the duration of the sporadic E-layer appearance.

12. Acronyms

EPP	Energetic Particle Precipitation
EISCAT	European Incoherent Scatter Scientific Association
OH	hydroxyl
IPY	International Polar Year
KHO	Kjell Henriksen-Observatory
IMF	Interplanetary Magnetic Field
NOAA	National Oceanic and Atmospheric Administration
TIMED	Thermosphere Ionosphere Mesosphere Energetics and Dynamics
ICME	Interplanetary Coronal Mass Ejection
ESR	EISCAT Svalbard Radar
ESIRI	ESR Ionospheric D-Region Experiment for Investigation of EPP
NASA	National Aeronautics and Space Administration
UT	Universal Time
SABER	Sounding of the Atmosphere Using Broadbandemission Radiometry

A. APPENDIX

A.1. ESIRI experiment

A. APPENDIX

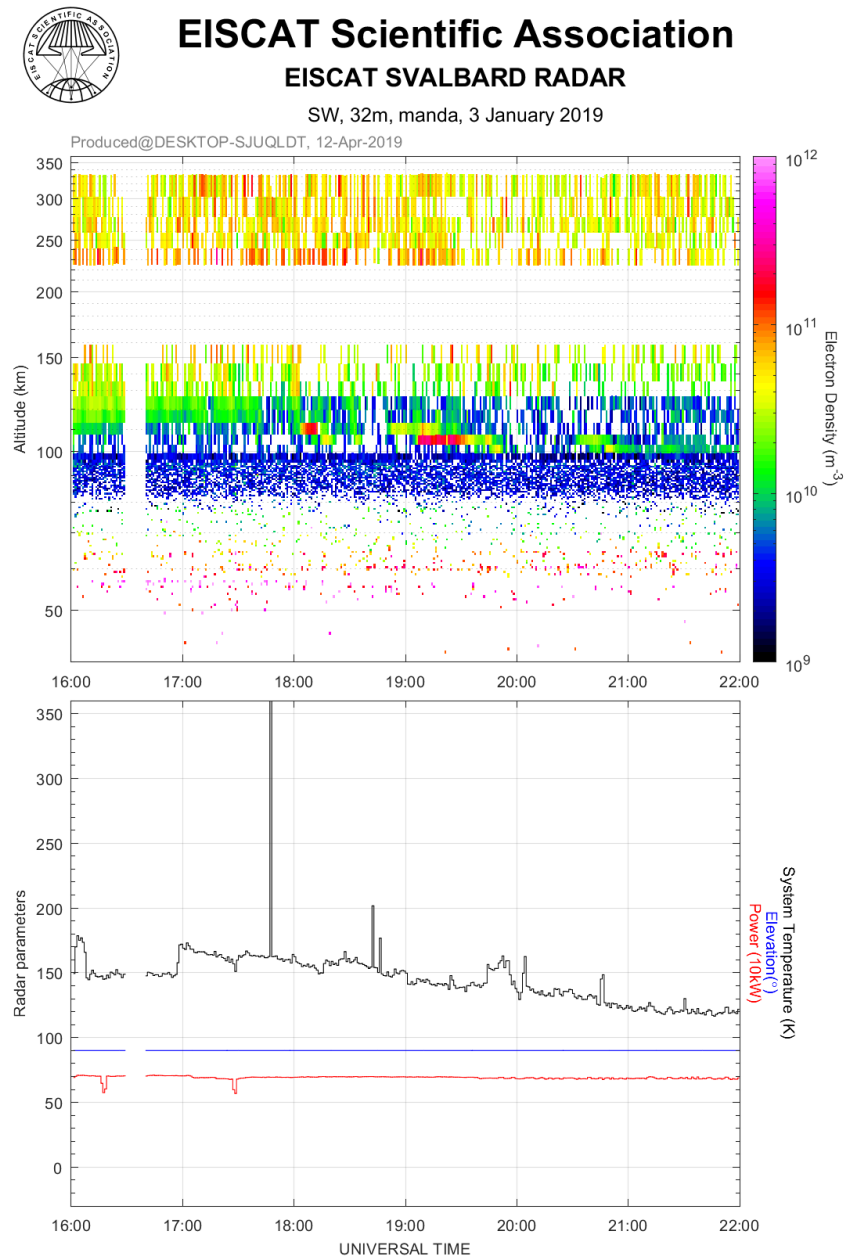


Figure A.1.: manda experiment on the 3rd of January 2019, 1600-2200 UT

A. APPENDIX

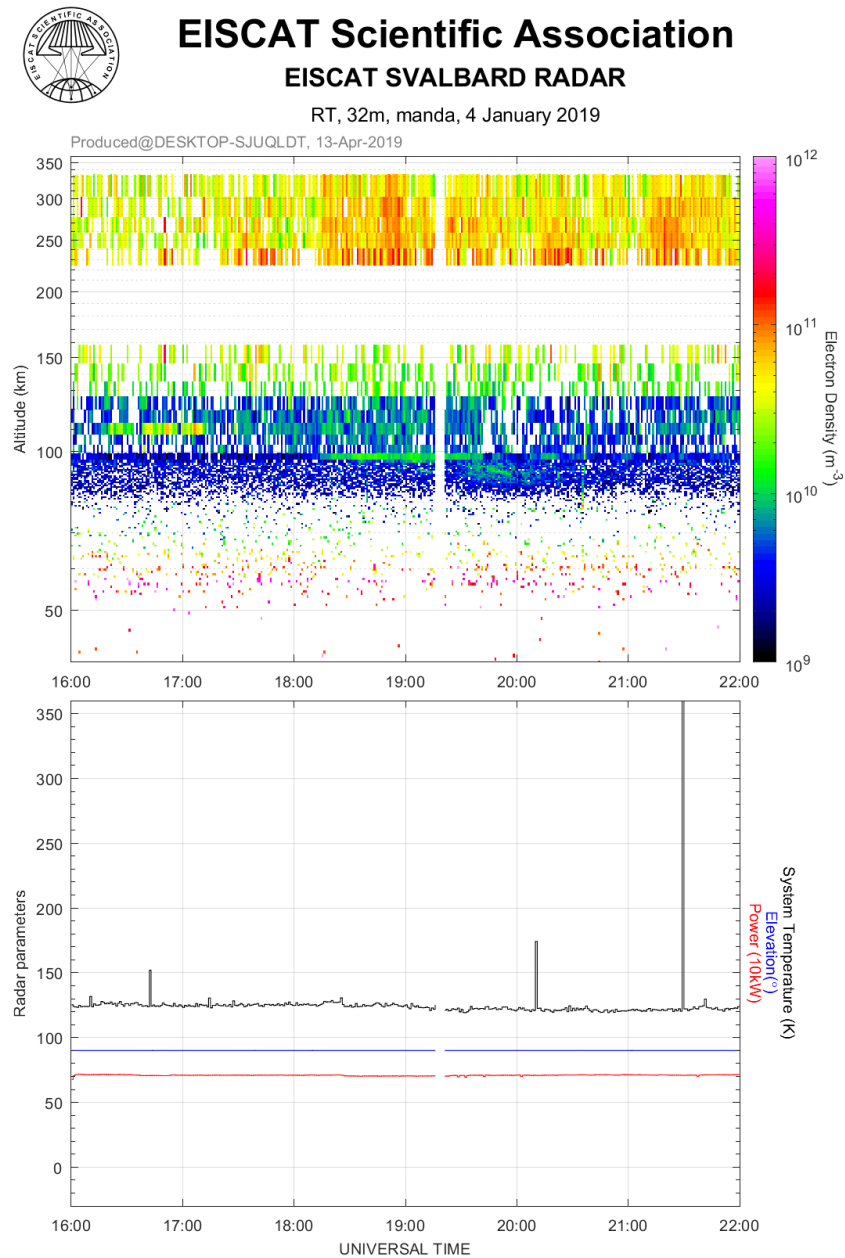


Figure A.2.: manda experiment on the 4th of January 2019, 1600-2200 UT

A. APPENDIX

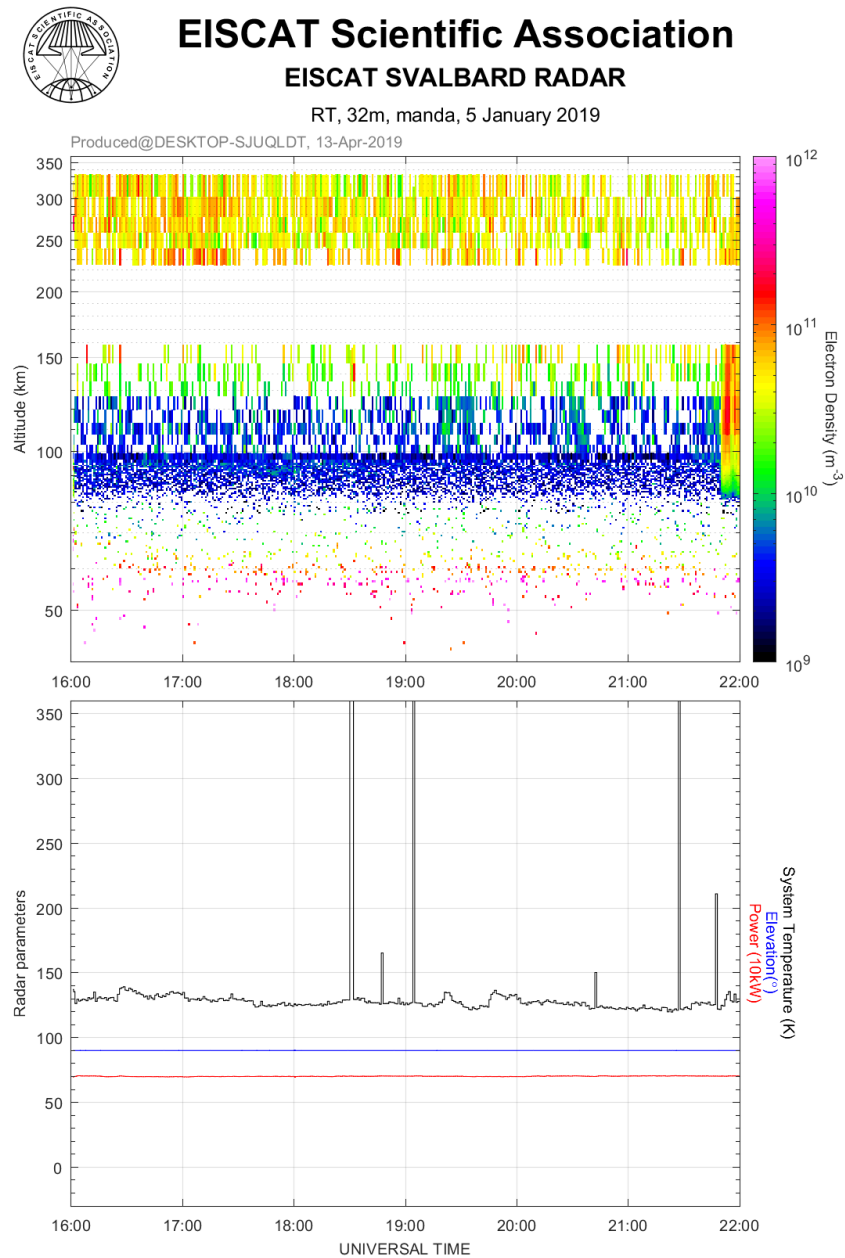


Figure A.3.: manda experiment on the 5th of January 2019, 1600-2200 UT

A. APPENDIX

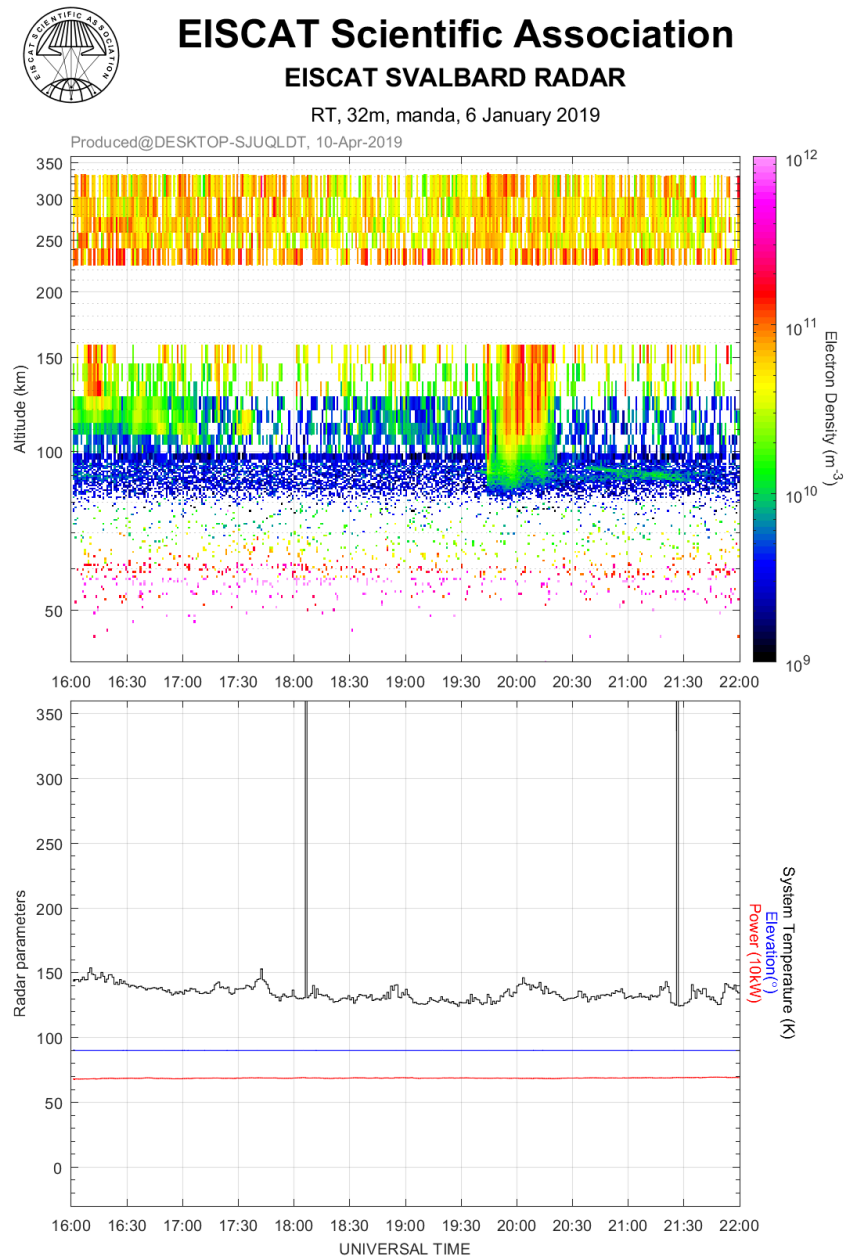


Figure A.4.: manda experiment on the 6th of January 2019, 1600-2200 UT

A. APPENDIX

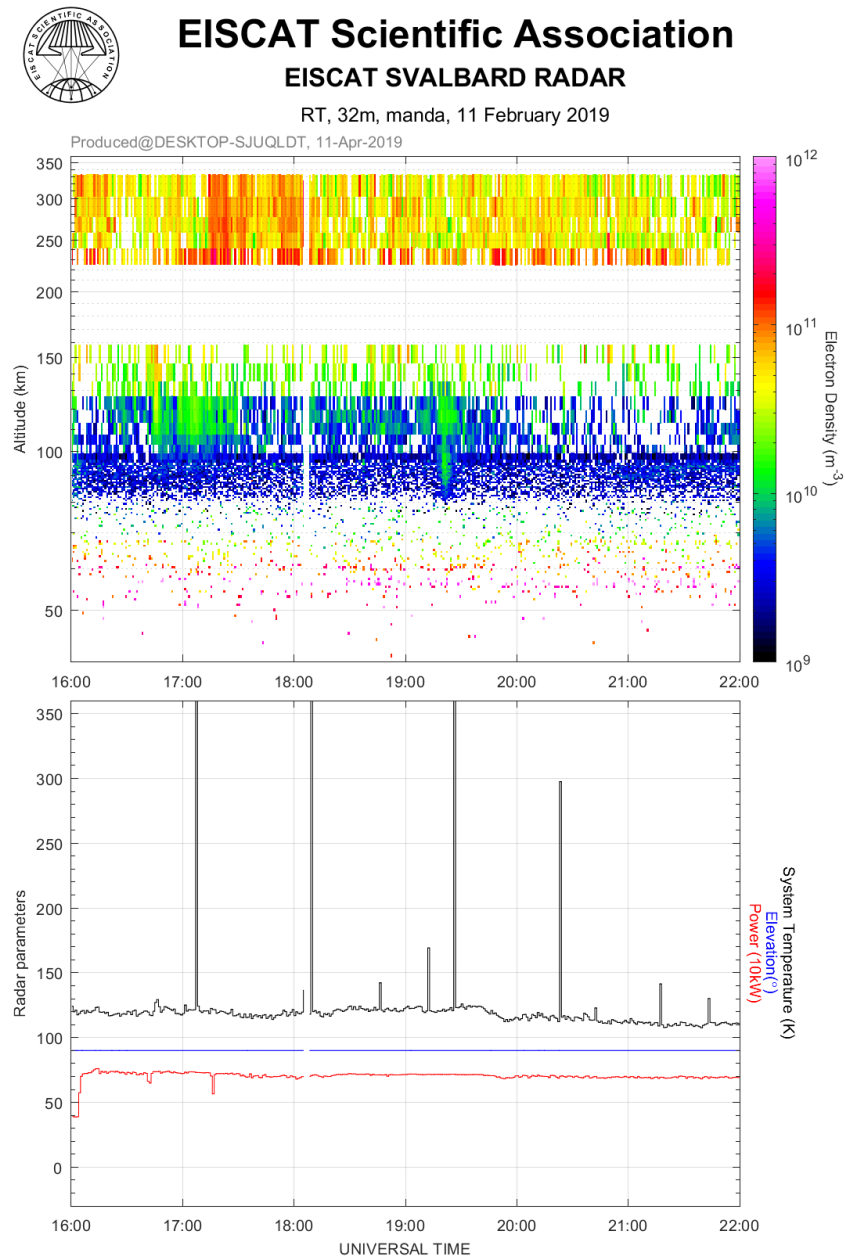


Figure A.5.: manda experiment on the 11th of February 2019, 1600-2200 UT

A. APPENDIX

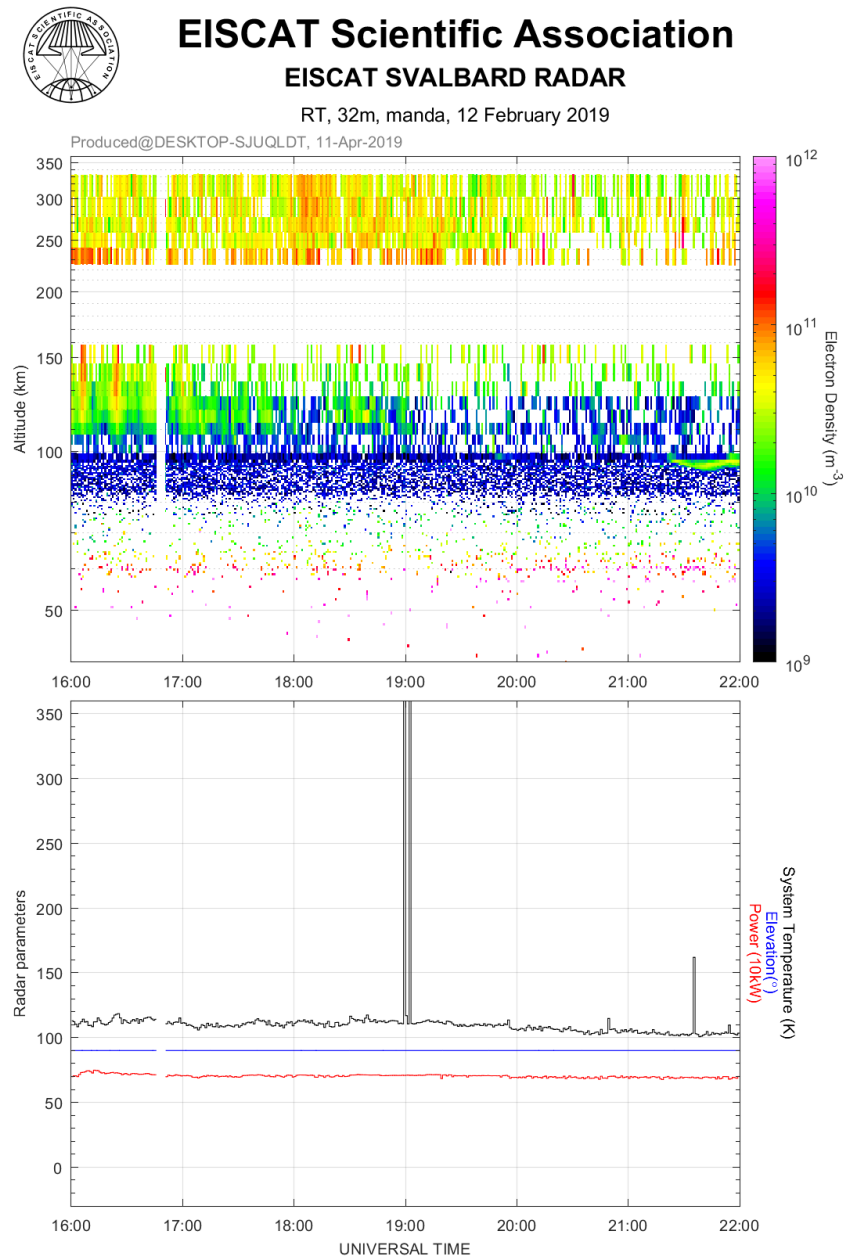


Figure A.6.: manda experiment on the 12th of February 2019, 1600-2200 UT

A. APPENDIX

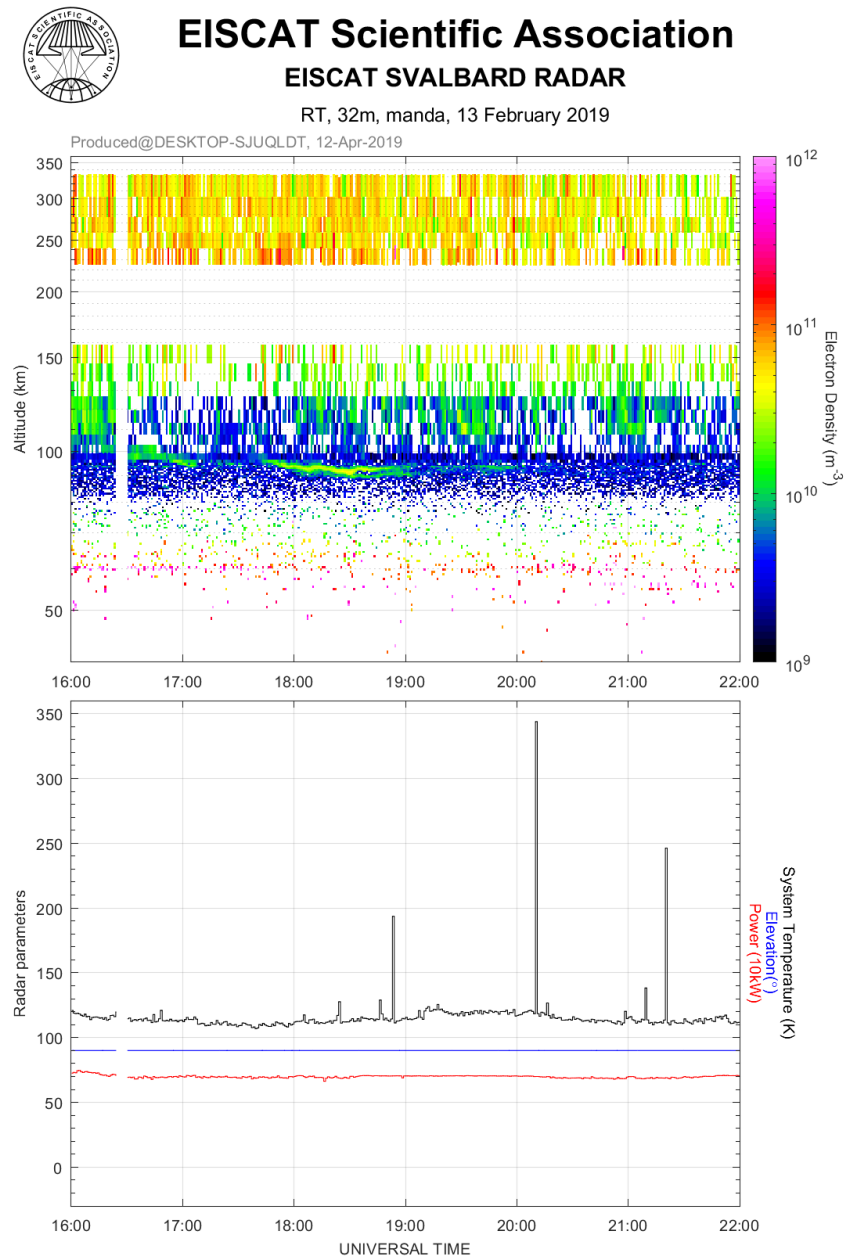


Figure A.7.: manda experiment on the 13th of February 2019, 1600-2200 UT

A. APPENDIX

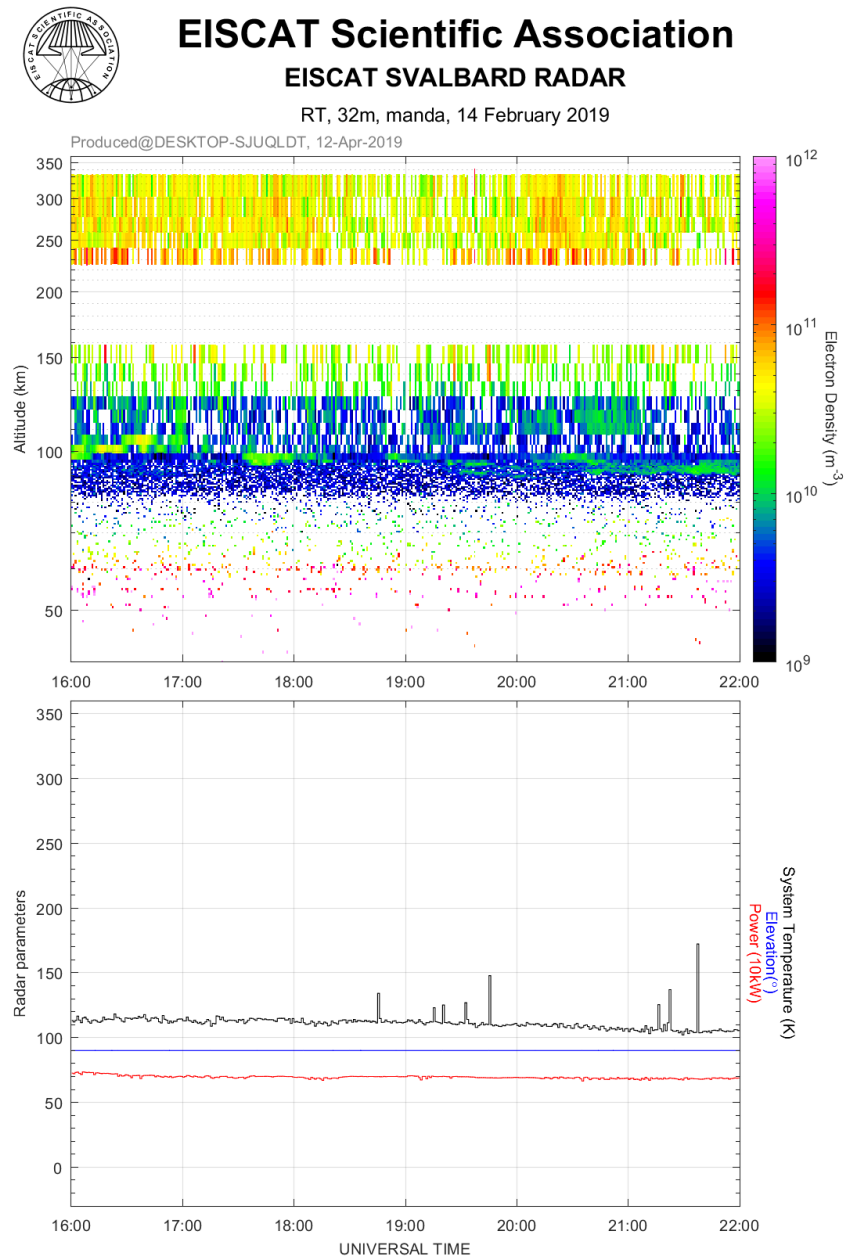


Figure A.8.: manda experiment on the 14th of February 2019, 1600-2200 UT

A.2. Matlab codes

A.2.1. Reading in the EISCAT Data

```
1 %%%%% main: loading EISCAT data
2
3
4 %%%% season 20xx/xx
5
6 %% choose altitudes to import
7 h = [87:1:94]'; \h stands for heights
8 dh=1; \height steps
9
10 %%% initializing electron density, error, time empty
11 Ne = [];
12 t = [];
13 Ne_error = [];
14
15 %% call function for electron density Ne, azimuth radar r_az, elevation
16 %% radar r_el, altitude range radar r_h, electron density error Ne_error,
17 %% radar files time steps t, read in .mat EISCAT GUISDAP files
18
19
20 [Ne,r_az,r_el, r_h,r_param,Ne_error,t] = readinEISCATraw(h,t);
21
22 %% time, thelp shows minutewise timesteps from the full hour on when the
23 %% data recording started until + 7 min for averaging purposes
24
25 minu=datenum(0,0,0,0,1,0);
26 begin=datevec(t(1));
27 t1=datenum(begin(:,1),begin(:,2),begin(:,3),begin(:,4),0,0);
28 smin=datenum(0,0,0,0,7,0);
29 tend=t(end)+smin;
30 thelp = t1:minu:tend;
31
32 %% create an electron density matrix for all times with NaNs
33 [newNe,newError] = createnewNe(Ne,h,t,thelp,minu,Ne_error);
34
35 %% average over heights, create new height range
36 [newhNe,newh,newhErr]=createheightaverage(newNe,h,thelp,newError)
37
38 %% make a ten min average
39 [meanNe,time,meanErr] = createmeanNe(newhNe,newh,thelp,newhErr);
40 showdates = datevec(time);
41 height=newh;
42
43 %% save .mat file with the data for the full year
44 save('D:\thesis\season1011\allseasonanalyse\EISCATtomatlab\1011-ipymat','time','r_param','r_el','r_az',
      'meanNe','height','dh','meanErr')
```



```
1 %%% function to read in the EISCAT data
2
```

A. APPENDIX

```
3 function [Ne,r_az,r_el, r_h,r_param,Ne_error,t] = readinEISCATraw(h,t)
4
5 directory = 'D:\thesis\season1011\IPY_analysisfiles';
6 warning off
7 disp(['Loading EISCAT MAT-files from ',directory])
8 matfiles = dir(fullfile(directory,'*','*.mat'))
9 disp([' Identified ',num2str(length(matfiles)), ' files'])
10
11 for i=1:length(matfiles)
12     load(fullfile(matfiles(i).folder, matfiles(i).name));
13
14 %%% last full minute timestep for each file is stored
15
16 t(i)= datenum(r_time(2,1),r_time(2,2),r_time(2,3),r_time(2,4),r_time(2,5),0);
17
18 %%% only heights within the predefined range are read in
19
20 for k=1:length(h)
21     ih = find(r_h > h(k)-0.5 & r_h < h(k)+0.5);
22
23     if isempty(ih)
24         Ne(k,i) = NaN;
25         Ne_error(k,i) = NaN;
26     elseif length(ih)>1
27         Ne(k,i)=mean(r_param(ih,1));
28         Ne_error(k,i) = mean(r_error(ih,1));
29     else
30
31         Ne(k,i) = r_param(ih,1);
32         Ne_error(k,i) = r_error(ih,1);
33     end
34 end
35 end
36 end
```

```
1 %%% function to create a new Ne and Ne error matrix
2 function [newNe,newError] = createnewNe(Ne,h,t,thelp,minu,Ne_error)
3
4 %%% store Ne for every minute otherwise set NaN
5
6 minh=minu*0.5;
7 newNe(1:length(h),1:length(thelp)) = NaN;
8 newError(1:length(h),1:length(thelp)) = NaN;
9
10 tdatevec= datevec(t);
11 timedatevec= datevec(thelp);
12
13 for w = 1:length(t)
14     it = find(thelp < t(w)+ minh & thelp > t(w)- minh);
15     newNe(:,it)= Ne(:,w);
16     newError(:,it)= Ne_error(:,w);
17 end
18 end
```

A. APPENDIX

```
1 %% function to create a mean Ne and mean Ne error matrix
2 function [meanNe,time,meanErr] = createmeanNe(newhNe,newh,thelp,newhErr)
3
4 time = [];
5 meanNe = [];
6 mNt= [];
7
8 datevec(thelp);
9
10 %% minutewise, start at minute ten, go in steps of ten
11 for x=11:10:length(thelp)-10
12     meanindex=(x-1)/10;
13     tindex = thelp > thelp(x-5)& thelp < thelp(x+6);
14     for p=1:length(newh)
15         mNt = newhNe(p,tindex);
16         mEt = newhErr(p, tindex);
17         meanNe(p,meanindex) = mean(mNt,'omitnan');
18         meanErr(p,meanindex) = mean (mEt, 'omitnan');
19     end
20     time(meanindex) = thelp(x);
21 end
```

```
1 %% function to create a height average
2 function [newhNe,newh,newhErr] = createheightaverage(newNe,h,thelp,newError)
3 newh=zeros;
4 newhNe=zeros;
5 k=4;
6 step=1;
7 for u=3:k:length(h)
8     x = (u+step)/k;
9     for v=1:length(thelp)
10        specNe = newNe(u-step-1:u+step,v);
11        specErr = newError(u-step-1:u+step,v);
12        newhNe(x,v) = mean(specNe,'omitnan');
13        newhErr(x,v) = mean(specErr,'omitnan');
14        newh(x)= h(u);
15    end
16 end
17 end
```

A.2.2. Finding the Events

```
1 %%%% main: finding the events
2
3 %% enter path to load the .mat data for year 20xx/xx
4 load('D:\thesis\seasonxxxx\allseasonanalyse\EISCATtomatlab\xxxx-ipy.mat');
5 h=height;
6 t=time;
7
8 %% find substorm like events, store them as time vector of events in
9 %% altitude 1 (87 – 90 km) t_ev_a1 and time vector of events in
10 %% altitude 2 (91 – 94 km) t_ev_a2
11
```

A. APPENDIX

```
12 [t_ev_a1,ec1,t_ev_a2,ec2] = findevents(h,t,meanNe);
13
14 %%% datevector for substorm events
15 showd1=datevec(t_ev_a1);
16 showd2=datevec(t_ev_a2);
17
18 %%% filter substorm like events (no events that are only 10 min apart)
19 [sortedeventsa1, sortedeventsa2] = filterevents(t_ev_a1, t_ev_a2);
20
21 %%% datevector for sorted substorm events
22 showsea1=datevec(sortedeventsa1);
23 showsea2=datevec(sortedeventsa2);
24
25 %%% savefile as txt. file
26 savefiles(showsea1, showsea2);
27
28 %%% save .mat file
29 save ('substromevents1.mat', 'sortedeventsa1','h')
30 save ('substromevents2.mat', 'sortedeventsa2','h')
```

```
1 %%%%%% function to find the events
2
3 function [t_ev_a1,ec1,t_ev_a2,ec2,t_ev_a3,ec3] = findevents(h,t,meanNe)
4 t_ev_a1 = []; %initialize empty time arrays
5 t_ev_a2 = [];
6
7 ec1=0; %eventcount for altitude 1
8 ec2=0; %eventcount for altitude 2
9
10 %%% choose mean Ne threshold to register as an event: increase of 4 times
11 %%% preceding mean Ne level in the time step later or two time steps later
12
13 for i=1:size(meanNe,2)-2
14 if meanNe(1,i) > 0.5e+9
15 if meanNe(1,i+1)>4*meanNe(1,i)
16 t_ev_a1 = [t_ev_a1,t(i+1)];
17 ec1 = ec1+1;
18 elseif meanNe(1,i+2)>4*meanNe(1,i)
19 t_ev_a1 = [t_ev_a1,t(i+2)];
20 ec1 = ec1+1;
21 end
22 end
23 if meanNe(2,i) > 0.5e+9
24 if meanNe(2,i+1)>4*meanNe(2,i)
25 t_ev_a2 = [t_ev_a2,t(i+1)];
26 ec2 = ec2+1;
27 elseif meanNe(2,i+2)>4*meanNe(2,i)
28 t_ev_a2 = [t_ev_a2,t(i+2)];
29 ec2 = ec2+1;
30 end
31 end
32 end
```

A. APPENDIX

```
1 %%%%%% function to find the events
2
3 function [sortedeventsa1, sortedeventsa2] = filterevents(t_ev_a1, t_ev_a2)
4
5 %%% filter out double events
6
7 temp= [];
8
9 tstep= datenum(0,0,0,0,10,0);
10
11 %% tstep=0.0069;
12
13 check1= isempty(t_ev_a1);
14 check2= isempty(t_ev_a2);
15 if check1 == 0
16     sortedeventsa1 = [t_ev_a1(1)];
17 for k=2:length(t_ev_a1)-1
18     temp = t_ev_a1(k) - t_ev_a1(k-1);
19
20 if temp > 0.007
21     sortedeventsa1 = [sortedeventsa1;t_ev_a1(k)];
22 end
23 end
24 else
25     sortedeventsa1=NaN;
26 end
27
28 if check2 == 0
29     sortedeventsa2 = [t_ev_a2(1)];
30 for k=2:length(t_ev_a2)-1
31     temp = t_ev_a2(k) - t_ev_a2(k-1);
32
33 if temp > 0.007
34     sortedeventsa2 = [sortedeventsa2;t_ev_a2(k)];
35 end
36 end
37 else
38     sortedeventsa2=NaN;
39 end
40 end
41
42 %%%% code to save .txt files
43
44 function savefiles(showsea1, showsea2)
45
46 list=fopen('eventlist_substorms_a1.txt','w');
47 for a=1:size(showsea1,1)
48     for l=1:6
49         fprintf(list,'%d\t\t',showsea1(a,l));
50     end
51     fprintf(list,'\n',showsea1(a));
52 end
```

```

53 list=fopen('eventlist_substorms_a2.txt','w');
54 for b=1:size(showsea2,1)
55     for k=1:6
56         fprintf(list,'%d\t\t',showsea2(b,k));
57     end
58     fprintf(list,'\n',showsea2(a));
59 end

```

A.2.3. Electron Density and Airglow Temperature Event Plots

```

1 %%%%%% main: Ne and T event plots
2
3 %%% call function to read in the airglow
4 [airglowtime,Temperature,T_error,ohadapted] = readinairglow;
5
6 %%% call function to read in the radar data
7 [iairglow,t,meanNe,h,Ne_error] = readinradardata(airglowtime);
8
9
10 %% load events in for altitude 1 or altitude 2
11 load ('D:\thesis\seasonxxxx\allseasonanalyse\x4\findeventslist\substormevents1.mat');
12 ev= sortedevents1;
13
14 %% find the data +- 3 h around the event and plot it
15
16 %% run through event list
17 for x=1:length(ev)
18     tofevent=ev(x);
19     %% choose in which range to search for points, hourly range
20     thr = datenum(0,0,0,1,0,0);
21     %% eventindexrange for airglow T
22     eia = find(airglowtime >= tofevent - 3*thr & airglowtime <= tofevent + 3*thr);
23     %% eventindexrange for Ne
24     eiNe = find(t(:) >= tofevent - 3*thr & t(:) <= tofevent + 3*thr);
25     check1 = isempty(eia);
26     check2 = isempty(eiNe);
27     ticks = tofevent-4*thr :thr: tofevent+4*thr;
28
29     %% check that no vector is empty, only plot when there is data
30     if check1 == 0 && check2 == 0
31
32         %% table to double check data points
33         t1= table(datevec(t(eiNe)),meanNe(1,eiNe)');
34         %% (1,eiNe) for altitude 1 (2,eiNe) for altitude 2
35         t2=table(airglowtime(eia),ohadapted(eia,7))
36
37         figure (x)
38             subplot(2,1,1);
39             errorbar(t(eiNe),meanNe(1,eiNe),Ne_error(1,eiNe), '.')
40             %% (1,eiNe) for altitude 1 (2,eiNe) for altitude 2
41             xticks([ticks])
42             dateFormat=15; % 6 = mm/dd, 7 = dd, 5 = mm
43

```

A. APPENDIX

```
44 datetick('x',dateFormat,'keepticks')
45 xlabel('time [hh:mm]')
46 ylabel('electron density [m^-^3]')
47 ylim([0,10e10]);
48 hold on
49 plot([torefevent,torefevent],[0,10e10])
50 hold off
51
52 subplot(2,1,2);
53 errorbar(airglowtime(eia),ohadapted(eia,7),ohadapted(eia,8), 'r')%
54 xlabel('time [hh:mm]')
55 ylabel('temperature [K]')
56 xticks([ticks])
57 dateFormat=15; % 6 = mm/dd, 7 = dd, 5 = mm
58 datetick('x',dateFormat,'keepticks')
59 ylim([160, 270]);
60 hold on
61 plot([torefevent,torefevent],[160, 270])
62 hold off
63 formatOut= 30;
64
65 %%% choose altitude 1 a1 or altitude 2 a2 to save as .png
66 name = datestr(torefevent,formatOut);
67 filename = sprintf('a1%0s.png',name);
68 saveas(figure(x),filename);
69 end
70 end

1 %%%%%% function to read in the airglow data file with half hour resolution
2
3 function [airglowtime,Temperature,T_error,ohadapted] = readinairglow(~)
4
5 %%% load airglow data file
6 ohxxxx= load('D:\thesis\seasonxxxx\half_hourly_xx_v3.dat');
7 ohadapted=ohxxxx;
8 ohadapted(end,:)= [];
9
10 %%% adapt airglow list to center times
11 for j=1:length(ohadapted)
12 if ohadapted(j,5) > 55
13 ohadapted(j,5)=45;
14 ohadapted(j,6)=0;
15
16 elseif ohadapted(j,5) < 6
17 if ohadapted(j,4)~=0
18 ohadapted(j,4)=ohadapted(j,4)-1;
19 else
20 ohadapted(j,4)=23;
21 end
22 ohadapted(j,5)=45;
23 ohadapted(j,6)=0;
24
25 elseif ohadapted(j,5) > 5 && ohadapted(j,5) < 16
```

A. APPENDIX

```
26 if ohadapted(j,4)~=0
27     ohadapted(j,4)=ohadapted(j,4)-1;
28 else
29     ohadapted(j,4)=23;
30 end
31 ohadapted(j,5)=55;
32 ohadapted(j,6)=0;
33
34 elseif ohadapted(j,5) > 15 && ohadapted(j,5) < 26
35     ohadapted(j,5)=05;
36     ohadapted(j,6)=0;
37
38 elseif ohadapted(j,5) > 25 && ohadapted(j,5) < 36
39     ohadapted(j,5)=15;
40     ohadapted(j,6)=0;
41
42 elseif ohadapted(j,5) > 35 && ohadapted(j,5) < 46
43     ohadapted(j,5)=25;
44     ohadapted(j,6)=0;
45
46 elseif ohadapted(j,5) > 45 && ohadapted(j,5) < 56
47     ohadapted(j,5)=35;
48     ohadapted(j,6)=0;
49 end
50 end
51 Temperature=ohadapted(:,7);
52 T_error=ohadapted(:,8);
53 airglowtime=datenum(ohadapted(:,1),ohadapted(:,2),ohadapted(:,3),ohadapted(:,4),ohadapted(:,5),0);
54 end
```

```
1 %%%%%% function to read in the airglow data file with hourly resolution
2
3 function [airglowtime,Temperature,T_error,ohadapted] = readinairglow(~)
4
5 ohxxxx= load('D:\thesis\seasonxxxx\hourly_xxxx_v2.dat');
6 ohadapted=ohxxxx;
7 ohadapted(end,:)= [];
8
9 %%% adapt airglow list to centered times
10 for j=1:length(ohadapted)
11     if ohadapted(j,5) > 55
12         ohadapted(j,5)=30;
13         ohadapted(j,6)=0;
14
15 elseif ohadapted(j,5) < 6
16     if ohadapted(j,4)~=0
17         ohadapted(j,4)=ohadapted(j,4)-1;
18     else
19         ohadapted(j,4)=23;
20     end
21     ohadapted(j,5)=30;
22     ohadapted(j,6)=0;
23
```

A. APPENDIX

```
24 elseif ohadapted(j,5) > 5 && ohadapted(j,5) < 16
25     if ohadapted(j,4)~=0
26         ohadapted(j,4)=ohadapted(j,4)-1;
27     else
28         ohadapted(j,4)=23;
29     end
30     ohadapted(j,5)=40;
31     ohadapted(j,6)=0;
32
33 elseif ohadapted(j,5) > 15 && ohadapted(j,5) < 26
34     if ohadapted(j,4)~=0
35         ohadapted(j,4)=ohadapted(j,4)-1;
36     else
37         ohadapted(j,4)=23;
38     end
39     ohadapted(j,5)=50;
40     ohadapted(j,6)=0;
41
42 elseif ohadapted(j,5) > 25 && ohadapted(j,5) < 36
43     ohadapted(j,5)=00;
44     ohadapted(j,6)=0;
45
46 elseif ohadapted(j,5) > 35 && ohadapted(j,5) < 46
47     ohadapted(j,5)=10;
48     ohadapted(j,6)=0;
49
50 elseif ohadapted(j,5) > 45 && ohadapted(j,5) < 56
51     ohadapted(j,5)=20;
52     ohadapted(j,6)=0;
53 end
54 end
55
56 Temperature=ohadapted(:,7);
57 T_error=ohadapted(:,8);
58 airglowtime=datenum(ohadapted(:,1),ohadapted(:,2),ohadapted(:,3),ohadapted(:,4),ohadapted(:,5),0);
59 end
```

```
1 %%% function to read in the .mat prepared radar data
2
3 function [iairglow,t,meanNe,h,Ne_error] = readinradardata(airglowtime)
4
5 %%% load in the radar prepared data
6 load('D:\thesis\seasonxxxx\allseasonanalyse\EISCATtomatlab\xxxx-ipy.mat');
7
8 %%% indices of at which electron density values the airglow temperature
9 %% value is available
10 iairglow=[];
11 t=time;
12 h=height;
13 %%% t(iag) indices of t when there is an airglow registered
14 %% time= airglow event
15
16 for s=1:length(airglowtime)
```

```

17     itemp = find(t == airglowtime(s));
18     iairglow = [iairglow;itemp];
19 end
20
21 Ne_error=meanErr;
22
23 %% preparation to have non zero values in the mean electron density
24 %% values
25 for o=1:size(meanNe,2)
26     for k=1:size(meanNe,1)
27         if meanNe(k,o) <= 0
28             meanNe(k,o) = NaN;
29         end
30     end
31 end

```

A.2.4. Scatter Plot

```

1 %% read in all radar data and all events
2 [airglowtime,Temperature,T_error,meanED,meanNe_error,Netime] = readindata;
3 [eventarrays] = readinevents;
4
5 %% scatter plot
6 for x=1:length(eventarrays)
7     tofevent=eventarrays(x); %% run through events
8     %% choose in which range to search for points, hourly range
9     thr = datenum(0,0,0,1,0,0);
10    eia = find(airglowtime >= tofevent - 1*thr & airglowtime <= tofevent + 2*thr); %% eventindexrange
11
12    %% average the Ne (choose hourly averaging or no averaging within the function)
13    [hourlyNe,hNetime] = averageNe(eia,airglowtime,Netime,meanED,eventarrays,x);
14
15    figure(1)
16    scatter(Temperature(eia), hourlyNe,'filled','b')
17    axis xy
18    xlabel('temperature [K]');
19    ylabel('electron density [m^-^3]');
20    hold on
21
22 end

```

```

1 %%% function to read in the .mat files
2 function [airglowtime,Temperature,T_error,meanED,meanNe_error,Netime] = readindata(~)
3 %% specify from which class directory to read in the data
4 directory = 'D:\thesis\event_plots\cases x4\T_gaps\scatter_plots\code';
5 matfiles = dir(fullfile(directory, '*', '*.mat')) % >= Matlab R2016b !!!
6 disp([' Identified ',num2str(length(matfiles)), ' files'])
7
8 meanED=[];
9 meanNe_error=[];
10 Temperature=[];
11 T_error=[];
12 airglowtime=[];

```

A. APPENDIX

```

13 Netime=[];
14 for i=1:length(matfiles)
15     load(fullfile(matfiles(i).folder, matfiles(i).name));
16     meanED = [meanED,meanNe];
17     meanNe_error = [meanNe_error,Ne_error];
18     Temperature = [Temperature; ohadapted(:,7)];
19     T_error=[T_error; ohadapted(:,8)];
20     airglowtime=[airglowtime; datenum(ohadapted(:,1),ohadapted(:,2),ohadapted(:,3),ohadapted(:,4),ohadapted(:,5),0)]);
21     Netime= [Netime,t];
22 end
23
24 end

```

```

1 %%%%%% function to read in events (from different classes or
2 %%%combined)
3 function [eventarray] = readinevents(~)
4
5 load('D:\thesis\event_plots\cases x4\T_cases\scatter_plots\code\matcases\T_case_all_events.mat');
6
7 end

```

```

1 %%%%%% function to average the electron density
2 function [hourlyNe,hNetime] = averageNe(eia,airglowtime,Netime,meanED,eventarray,x)
3
4 %%%%%%average the Ne
5
6 hNetime=[];
7 hourlyNe=[];
8 fmin=datenum(0,0,0,0,6,0)
9 for i=1:length(eia)
10    index = find(Netime >= (airglowtime(eia(i))-fmin) & Netime <= (airglowtime(eia(i))+fmin))
11    first= index(1)-2;
12    last= index(1)+3;
13    range=meanED(eventarray(x,2),first:last);
14    mrange=max(range);
15    hourlyNe(i)=log10(mrange);
16    checkisempty(index);
17    if check == 0
18        hNetime(i)=Netime(index(1));
19    end
20 end

```

A.2.5. Superposed Epoch Plot

The functions readinevents and readindata are the same ones as in Appendix A.2.4.

```

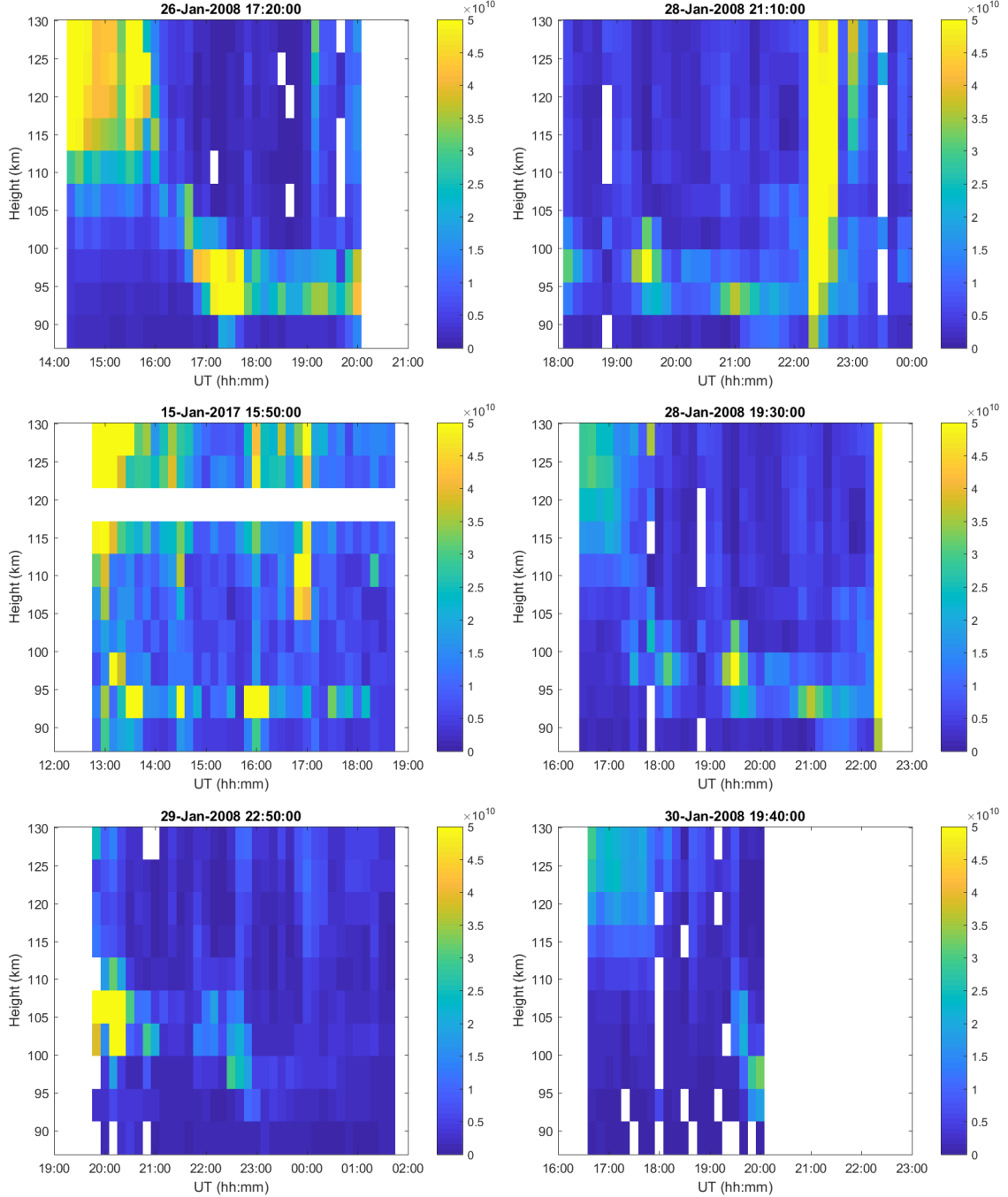
1 %% functions to read in events and data
2 [eventarray] = readinevents;
3 eventstart=datenum(eventarray(:,1));
4 [Temperature,airglowtime] = readindata;
5
6 airglowT=Temperature;

```

A. APPENDIX

```
7 t=airglowtime;
8 dt=datenum(0,0,0,1,0,0);
9 te_med=[];
10 ll=[];
11 h25=[];
12 h75=[];
13
14 %% choose which epoch to show (here: + - 4 h)
15 for p=4:-1:-4
16     mTe=[];
17     for i=1:length(eventstart)
18         t1=eventstart(i)-p*dt;
19         t2=eventstart(i)-(p-1)*dt;
20         tindex=find(t <= t2 & t >= t1);
21         if length(tindex)>0
22             tempTe=airglowT(tindex);
23             [xi,yi]=find(tempTe > 0);
24             mTe=[mTe; nanmean(tempTe(xi,yi))'];
25         end
26     end;
27     te_med=[te_med; nanmedian(mTe)];
28     ll=[ll; length(mTe)];
29     h25=[h25; prctile(mTe,25)];
30     h75=[h75; prctile(mTe,75)];
31 end; % p
32
33 %% Superposed epoch plot:
34 xx=-4:4;
35 hold on;
36 plot(xx,h25,'r-');
37 plot(xx,te_med,'b*-');
38 hold off
39 grid on
40 xlabel('epoch from EEP start [h]')
41 ylabel('temperature [K]')
```

A.3. Sporadic E-layer Events Electron Density Plots: Cases with Full Temperature Coverage (Hourly Resolution)



A. APPENDIX

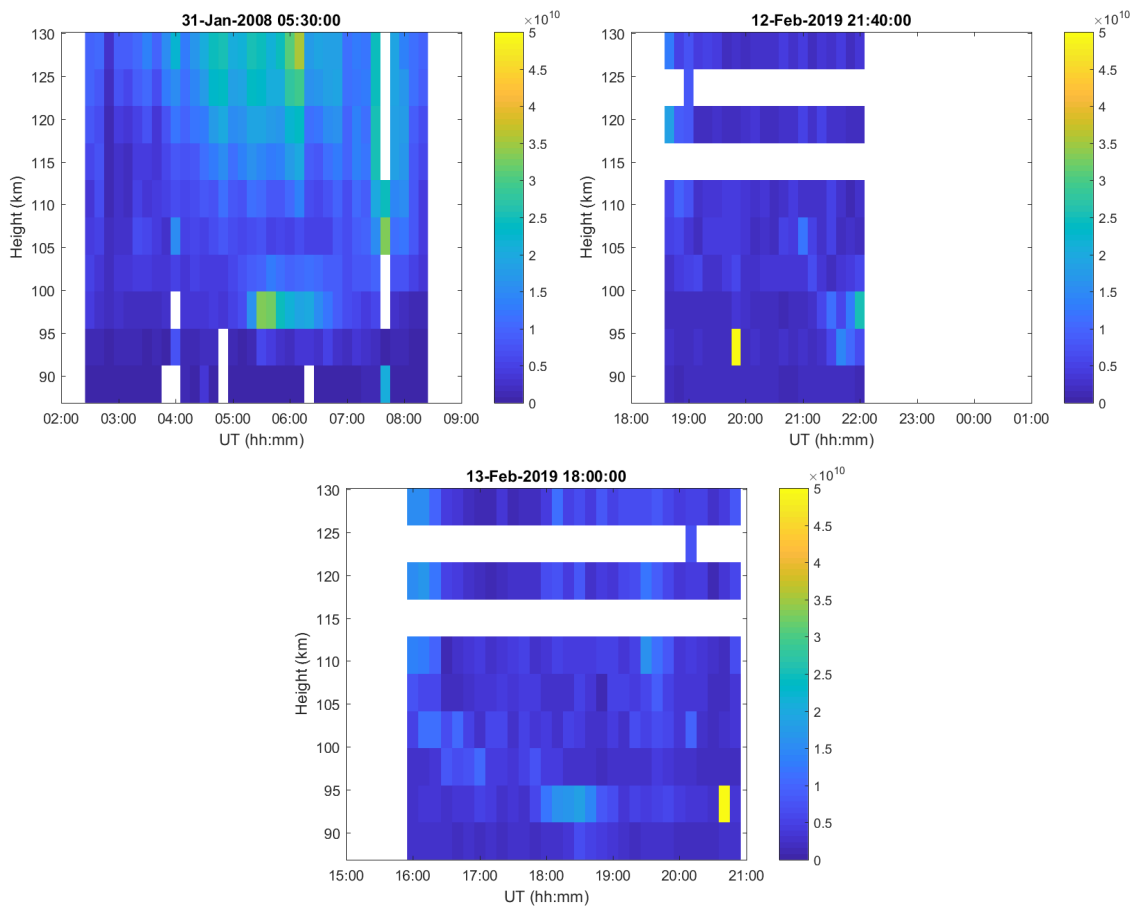


Figure A.9.: sporadic E-layer events, electron density plots versus altitude and time

Bibliography

- [1] *Heliophysical Processes*. Astrophysics and Space Science Proceedings. Springer Berlin Heidelberg, 2010. ISBN: 9783642113406.
- [2] D. G. Andrews. *An Introduction to Atmospheric Physics Second Edition*. CAMBRIDGE UNIVERSITY PRESS, 2010. ISBN: 9780511800788.
- [3] C. She and U. Von Zahn. "Concept of a two-level mesopause: support through new lidar observations". In: *Journal of Geophysical Research, Washington, DC* 103.D5 (1998), pp. 5855–5863. ISSN: 0148-0227. doi: 10.1029/97JD03450.
- [4] F. Mulligan, M. E. Dyrland, S. F, and C. S. Deehr. "Inferring hydroxyl layer peak heights from ground-based measurements of OH(6-2) band integrated emission rate at Longyearbyen (78 N, 16 E)". In: *Annales Geophysicae* 27 (Nov. 2009). doi: 10.5194/angeo-27-4197-2009.
- [5] A. Kivelson, M. Kivelson, and C. Russell. *Introduction to Space Physics*. Cambridge atmospheric and space science series. Cambridge University Press, 1995. ISBN: 9780521457149. URL: <https://books.google.com/books?id=qWHSqXGfsfQC>.
- [6] H. Nesse Tyssøy, J. Stadsnes, M. Sørbo, C. J. Mertens, and D. S. Evans. "Changes in upper mesospheric and lower thermospheric temperatures caused by energetic particle precipitation". In: *Journal of Geophysical Research: Space Physics* 115.A10 (2010). ISSN: 0148-0227. doi: 10.1029/2010JA015427.
- [7] H. Suzuki, M. Tsutsumi, T. Nakamura, and M. Taguchi. "The increase in OH rotational temperature during an active aurora event". In: *Annales Geophysicae* 28.3 (2010), pp. 705–710. doi: 10.5194/angeo-28-705-2010. URL: <https://www.ann-geophys.net/28/705/2010/>.
- [8] G. Gavrilova and P. Ammosov. "Influence of geomagnetic activity on mesopause temperature over Yakutia". In: *Atmospheric Chemistry and Physics* 18.5 (2018), pp. 3363–3367. doi: 10.5194/acp-18-3363-2018.
- [9] K.-H. Glameier, H. Soffel, and J. F. Negendank. *Geomagnetic Field Variations*. Advances in Geophysical and Environmental Mechanics and Mathematics. Berlin, Heidelberg: Springer Berlin Heidelberg, 2009. ISBN: 9783540769385.
- [10] H. Koskinen. *Physics of Space Storms*. 2011. ISBN: ISBN 978-3-642-00319-6. doi: 10.1007/978-3-642-00319-6.
- [11] F. A. Hanser and B. Sellers. "Pitch angle variation of auroral electrons slowing down in the upper atmosphere". In: *Planetary and Space Science* 21.11 (1973), pp. 2042–2043. ISSN: 0032-0633. doi: 10.1016/0032-0633(73)90133-5.

- [12] R. A. Marshall and J. Bortnik. "Pitch Angle Dependence of Energetic Electron Precipitation: Energy Deposition, Backscatter, and the Bounce Loss Cone". In: *Journal of Geophysical Research: Space Physics* 123.3 (2018), pp. 2412–2423. ISSN: 2169-9380. DOI: 10.1002/2017JA024873.
- [13] A. L. V. G. A. Kuck. "Induced precipitation of inner zone electrons, 1. Observations". In: *JGR Space Physics* 83.A6 (1978), pp. 2543–2551. ISSN: 00948276. DOI: 10.1029/JA083iA06p02543.
- [14] M. Rees. "Magnetospheric substorm energy dissipation in the atmosphere". In: *Planetary and Space Science* 23.12 (1975), pp. 1589–1596. ISSN: 0032-0633. DOI: 10.1016/0032-0633(75)90086-0.
- [15] J. Meriwether. "A review of the photochemistry of selected nightglow emissions from the mesopause". In: *Journal Of Geophysical Research-Atmospheres* 94.D12 (1989), pp. 14629–14646. ISSN: 2169-897X. DOI: 10.1029/JD094iD12p14629.
- [16] J. W. Chamberlain. *Physics of the Aurora and Airglow*. Washington, D. C.: American Geophysical Union, 2013. ISBN: 9781118668047.
- [17] M. C. E. H. L. J. L. D. Stoeffler. *Radio Techniques for Probing the Terrestrial Ionosphere*. Berlin, Heidelberg: Springer Berlin Heidelberg, 1991. ISBN: 9783642762598.
- [18] A. Tjulin. "EISCAT experiments". In: (2017). URL: <https://www.eiscat.se/wp-content/uploads/2016/05/Experiments.pdf>.
- [19] F. Sigernes, N. Shumilov, C. S. Deehr, K. P. Nielsen, T. Svenøe, and O. Havnes. "Hydroxyl rotational temperature record from the auroral station in Adventdalen, Svalbard (78N, 15E)". In: *Journal of Geophysical Research: Space Physics* 108.A9 (2003). ISSN: 0148-0227. DOI: /10.1029/2001JA009023.
- [20] M. E. Dyrland. <http://kho.unis.no/doc/airglowref.pdf>, 2010. ISBN: 9788282360142.
- [21] J. Mathews. "Sporadic E: current views and recent progress". In: *Journal of Atmospheric and Solar-Terrestrial Physics, Oxford, England* 60.4 (1998), pp. 413–435. ISSN: 1364-6826. DOI: 10.1016/S1364-6826(97)00043-6.
- [22] A. Pignalberi, M. Pezzopane, and E. Zuccheretti. "Sporadic E layer at mid-latitudes: average properties and influence of atmospheric tides". In: *Annales Geophysicae* 32.11 (2014). ISSN: 0992-7689. DOI: 10.5194/angeo-32-1427-2014.
- [23] "First experiences of full-profile analysis with GUISDAP". In: *Annales Geophysicae, European Geosciences Union* (1996), pp. 1487–1495. ISSN: 1432-0576. DOI: 10.1007/s00585-996-1487-3.
- [24] K. Cresswell-Moorcock, C. J. Rodger, A. Kero, A. B. Collier, M. A. Clilverd, I. Haggstrom, and T. Pitkanen. "A reexamination of latitudinal limits of substorm-produced energetic electron precipitation". In: *Journal of Geophysical Research. Space Physics* 118.10 (2013), pp. 6694–6705. ISSN: 21699380. DOI: 10.1002/jgra.50598.
- [25] K. Maeda. *The auroral O₂-dissociation and the infrared OH-emission*. Tech. rep. 1967. URL: <http://hdl.handle.net/2060/19670030065>.

Bibliography

- [26] M. Cooper. "Validation of SABER temperature measurements using ground-based instruments". In: *IGARSS 2004. 2004 IEEE International Geoscience and Remote Sensing Symposium* 6 (2004), pp. 4099–4101. issn: 0780387422. doi: 10.1109/IGARSS.2004.1368922.

